A&A manuscript no.
(will be inserted by hand later)

Your thesaurus codes are:
08.05.03, 08.22.1

ASTRONOMY
AND
ASTROPHYSICS

arXiv:astro-ph/9901294v1 21 Jan 1999

Period - luminosity - color - radius relationships of Cepheids as a function of metallicity: evolutionary effects.

Yann Alibert[1], **Isabelle Baraffe**[1,2], **Peter Hauschildt**[3], **and France Allard**[1]

[1] C.R.A.L (UMR 5574 CNRS), Ecole Normale Supérieure, 69364 Lyon Cedex 07, France
email: yalibert, ibaraffe, fallard @ens-lyon.fr
[2] Max-Planck Institut für Astrophysik, Karl-Schwarzschildstr.1, D-85748 Garching, Germany
[3] Dept. of Physics and Astronomy and Center for Simulational Physics, University of Georgia Athens, GA 30602-2451
email: yeti@hobbes.physast.uga.edu

Received /Accepted

Abstract. Based on consistent evolutionary and pulsation calculations, we analyse the effect of metallicity and of different convection treatments in the stellar models on period - magnitude, - color and - radius relationships. In order to perform an accurate comparison with observations, we have computed grids of atmosphere models and synthetic spectra for different metallicities, covering the range of effective temperatures and gravities relevant for Cepheids. The models are compared to recent observations of galactic and Magellanic Clouds Cepheids. Unprecedented level of agreement is found between models and observations.

We show that within the range of metallicity for the Galaxy and the Magellanic Clouds, a change of slope in the period - luminosity (PL) relationship is predicted at low periods, due to the reduction of the blue loop during core He burning. The minimum mass undergoing a blue loop and consequently the critical period at which this change of slope occurs depend on the metallicity Z and on the convection treatment in the stellar models.

However, besides this change of slope, we do not find any significant effect of metallicity on period - magnitude relationships from V to K bands, and on period - color relationships in IR colors. We only find a detectable effect of Z on $(B-V)$ colors. These results are not affected by uncertainties inherent to current stellar models, mainly due to convection treatment.

Key words: Cepheids – stars: evolution

1. Introduction

Although Cepheids have been studied extensively since the discovery by Leavitt in 1908 of their fundamental period - luminosity (PL) relationship, the metallicity dependence of this relation still remains unsettled (see Tanvir 1997 for a review). Since the Cepheid PL relationship is a cornerstone to extragalactic distance scales, the existence of such dependence is of fundamental importance.

This old debate has recently been revived due to high-quality observations from the HST, Hipparcos and the micro-lensing experiments which collected large samples of Cepheid data in the Magellanic Clouds (EROS: Renault et al. 1996, Beaulieu & Sasselov 1996 and references therein; MACHO: Welch et al. 1996 and references therein). The forthcoming release of the OGLE-2 data (Udalski, Kubiak, Szymanski 1997 and references therein) will bring further important elements to this debate. Based on the EROS Cepheid sample, a comparison of the observed PL relations in the Small (SMC) and the Large (LMC) Magellanic Clouds led Sasselov et al. (1997) to suggest a significant metallicity effect. In the same vein, Sekiguchi and Fukigita (1998) reanalysed Cepheid data used as calibrators and claimed also a large metallicity effect. Such controversy with previous claims (see Tanvir 1997) illustrates the difficulty to disentangle a metallicity effect from other effects such as reddening or distance uncertainties and to reach definitive conclusions.

Since empirical calibrations do not provide a clear answer to the metallicity correction, a theoretical analysis could provide the basis for a better understanding of this problem. However, uncertainties inherent to stellar evolution models (convection treatment, overshooting, opacities, etc..), pulsation calculations (nonlinear effects, time-dependent convection) and atmosphere models required to determine the bolometric corrections render the task difficult.

One of the most systematic study has been performed by Chiosi, Wood & Capitanio (1993), based on linear stability analysis of a large grid of models with different compositions, effective temperatures, masses and mass - luminosity (ML) relationships. The metallicity effect on the PL relationship was found to be rather small. However, the models of Chiosi et al. (1993) are based on the old Los Alamos opacity Library (Huebner et al. 1977), which

---

Send offprint requests to: Y. Alibert

is a key ingredient to the stellar and pulsation models. Since then, opacity calculations have greatly improved, thanks to both the Livermore group (OPAL, Iglesias & Rogers 1991; Iglesias, Rogers, & Wilson 1992) and the OP project (Seaton et al. 1994). More recently, Iglesias and Rogers (1996) have updated the OPAL opacities, with an increase of the opacity up to 20% for solar-type mixtures. Adopting these improved opacities, Saio and Gautschy (1998) derived theoretical PL relationships based on consistent stellar evolution and linear pulsation calculations for different metallicity and masses ranging from 4 to 10 $M_\odot$. They find a negligible metallicity dependence of the PL relationship. On the other hand, Bono et al. (1998a, BCCM98) recently investigated the PL and period - color (PC) relationships on the basis of non-linear calculations. Their analysis, which covers a mass range from 5 to 11 $M_\odot$ predicts a significant dependence of the PL relationship on metals, in contradiction with the results of Saio and Gautschy (1998), although for similar mass and metallicity ranges.

In parallel with the work of Saio and Gautschy (1998), Baraffe et al. (1998) performed self-consistent calculations between stellar evolution and linear stability analysis for the SMC, the LMC and the Galaxy. This work was mainly devoted to the comparison with the observed PL relationships and the Beat Cepheids of the SMC and LMC data obtained by the EROS and MACHO groups. Baraffe et al. (1998) have emphasized the importance of the first crossing instability phase, which corresponds to models which are just leaving the Main Sequence and evolving toward the Red Giant Branch on a thermal time-scale. Such models can explain most of the first-overtone/second-overtone (1H/2H) beat Cepheids observed in the Magellanic Clouds (MC). An other important result stressed in Baraffe et al. (1998) is the possible explanation by pure evolutionary effects of the change of slope in the PL relationship observed by Bauer et al. (1998) for short period SMC Cepheids. Such results show the necessity to take into account evolutionary properties in order to derive reliable PL relationships and reproduce observations.

The goal of the present paper is to analyse carefully the PL relationships based on the evolutionary models of Baraffe et al. (1998), taking into account the effect of chemical composition and of different convection treatments on the evolutionary models (§2). Baraffe et al. (1998) did not perform such detailed analysis, since their bolometric corrections were derived from atmosphere models with constant gravity. For the purpose of the present work, we have calculated a grid of atmosphere models covering the required range of effective temperatures and gravities and for the same metallicities as in the evolutionary models. This enables us to analyse fine effects of metallicity on the derived synthetic colors. In §3, we derive theoretical PL relationships and §4 is devoted to the comparison with observed period-magnitude-color-radius relationships in the SMC, LMC and the Galaxy. We construct also theoretical period histograms and compare them to the observed histograms derived from sample of Cepheids in the MC's (cf. §4). Finally, section 5 is devoted to the analysis of metallicity effects and to discussion and §6 to conclusions.

2. Evolutionary calculations

Stellar models are computed with the Lyon evolutionary Henyey-type code, originally developed at the Göttingen Observatory (Baraffe and El Eid 1991). The most recent OPAL opacities (Iglesias & Rogers 1996) are used for the inner structure $T > 6000K$. For temperatures lower than $6000K$, we use the Alexander & Fergusson (1994) opacities. Mass loss is taken into account according to de Jager et al. (1988) with a scaling factor which depends on the metallicity as $(Z/Z_\odot)^{0.5}$, as indicated by stellar wind models (Kudritzki et al. 1987, 1991). The effect of mass loss is however negligible during the evolutionary phases involved, and in any case the total mass lost does not exceed 2 % of the initial mass.

Convective transport is computed using the mixing-length theory formalism as given by Kippenhahn & Weigert (1990). The ratio $\alpha_{\rm mix}$ of the mixing length ($l_{\rm mix}$) to the pressure scale height ($H_{\rm P}$) is fixed to 1.5. In order to determine the uncertainties resulting from a variation of $l_{\rm mix}$, we have also computed two sets of evolutionary tracks with $\alpha_{\rm mix} = 2$ for metallicities representative of the MC's, for which more Cepheid data (fundamental and overtone pulsators) are available than for the Galaxy.

The onset of convective instability is based on the Schwarzschild criterion. Our main grid of evolutionary models is computed with standard input physics (e.g without overshooting, semiconvection, or rotation induced mixing). In order to test the effect of some enhanced mixing in the convective core, as expected when using overshooting, we have also computed models in which the size of the convective core is arbitrarily increased by an amount $d_{\rm ov} = \alpha_{\rm ov} H_{\rm P}$, where $\alpha_{\rm ov}$ is a free parameter fixed to 0.15, as justified in §2.3 and §4.5. This extended region is assumed to be completely mixed, but the temperature gradient is supposed to be radiative. This type of simple prescription is usually used to mimic the effect of overshooting or any other source of enhanced mixing beyond the standard convective boundary (cf. El Eid, 1994; Pols et al. 1998).

We have computed stellar models in the mass range $2.75 - 12 M_\odot$ with various chemical compositions $(Z, Y) = (0.02, 0.28)$, $(0.01, 0.25)$ and $(0.004, 0.25)$ [1], representative of respectively the Galactic, LMC and SMC environments. In the case of the LMC, we have also computed different grids of models with various Z and Y, *i.e.* $(Z, Y) = (0.01, 0.25)$, $(Z, Y) = (0.01, 0.28)$, and $(Z, Y) = (0.008, 0.25)$.

---

[1] Z is the metal mass fraction and Y the helium mass fraction

2.1. Effect of the initial chemical composition

Since the present paper is devoted to period - luminosity relationships rather than to stellar evolutionary models, we concentrate in the following on properties relevant to Cepheids. The first important effect of metallicity concerns the determination of the minimum mass m_{min} which undergoes a blue loop entering the instability strip (IS). As shown in Fig. 1, $m_{\rm min}$ decreases with metallicity. We find for the fundamental mode IS $m_{\rm min} \sim 3 M_\odot$ for Z=0.004, $m_{\rm min} \sim 3.875 M_\odot$ for Z=0.01 and $m_{\rm min} \sim 4.75 M_\odot$ for Z=0.02. Note that Baraffe et al. (1998) mention slightly lower $m_{\rm min}$ for Z=0.01 and Z=0.02, but as shown in §3, these lower values are too uncertain due to the arbitrary criterion used to determine the red edge. Fig. 1 displays the evolutionary tracks of stars of mass $m_{\rm min}$ for different metallicities and the location of fundamental unstable models (see §3 for the description of the linear stability analysis). Stars with masses just below $m_{\rm min}$ undergo a reduced blue loop which does not enter the instability strip. Note that all stellar models in Fig. 1 show fundamental unstable modes during the first crossing of the Hertzsprung-Russel diagram (HRD) toward the Red Giant Branch (see Baraffe et al. 1998 for details).

As shown in §3, determination of PL relationships is affected by the behavior of $m_{\rm min}$, since the reduction of the blue loop affects the width of the instability strip at short periods. Indeed, the blue edge (BE) is in this case determined by the turnover of the evolutionary track. Note that determination of blue edges based on stability analysis of envelope models constructed for a given mass - luminosity relationship and obtained by varying arbitrarily $T_{\rm eff}$ would predict a hotter BE for masses near $m_{\rm min}$. To illustrate this effect, we note that the fundamental BE determined by the blue loop extension of the 3 $M_\odot$ star with Z=0.004 is at $T_{\rm eff}$ = 5860 K, corresponding to P_0 = 1.2 days and $\log L/L_\odot$ = 2.384. However, for the same mass, luminosity and chemical composition, stability analysis performed on envelope models show that fundamental modes should be unstable up to $T_{\rm eff}$ = 6600 K and P_0 = 0.83 days.

The extension of the blue loop depends not only on the metallicity but also on the helium abundance. This is shown in Fig. 2 which displays the evolutionary tracks of 4 $M_\odot$ stars with respectively $(Z, Y) = (0.01, 0.25)$ (solid curve), $(Z, Y) = (0.008, 0.25)$ (dashed curve) and $(Z, Y) = (0.01, 0.28)$ (dotted curve). Since the size of the blue loop increases when Z decreases for a given mass near $m_{\rm min}$, we find $m_{\rm min}$ = 3.75 $M_\odot$ for $(Z, Y) = (0.008, 0.25)$, instead of 3.875 $M_\odot$ for Z=0.01 (independently of Y).

The final important effect of chemical composition to be mentioned in the present context concerns the mass - luminosity relationships. Since for decreasing metallicity, the luminosity during core helium burning increases for a given mass, this effect has to be taken into account in order to correctly analyse the metallicity dependence of PL relationships. Figure 3 shows the ML relationships based on the present standard calculations during the first crossing phase and during the blue loop from $m_{\rm min}$ to 10 $M_\odot$[2]. To estimate the following relationships, we have taken simple means of L in the instability strips (of F, 1H and 2H modes). We stress above all that these relationships illustrate the metallicity effect; more accurate values are given in the tables at the end of the present paper (Tables 6-8). During the first crossing phase we find the following relationships:

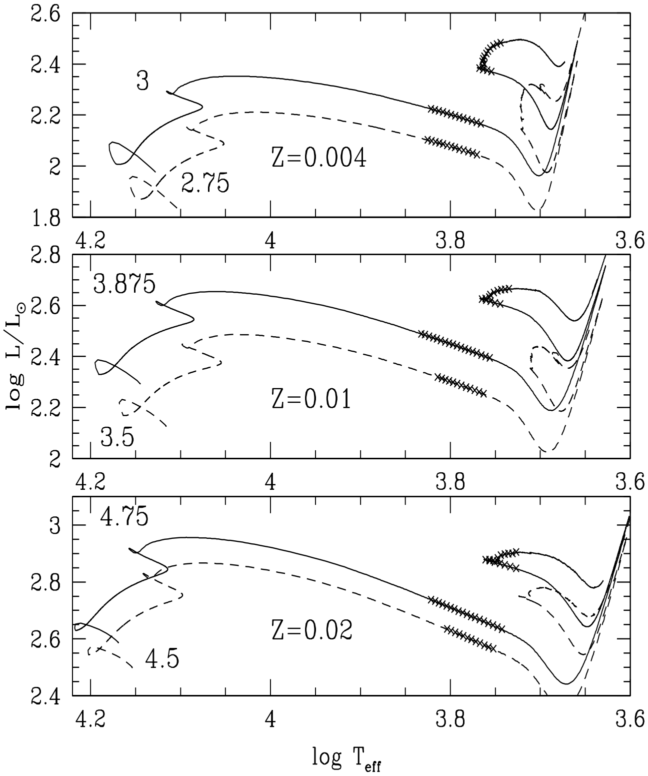

Fig. 1. Stellar evolutionary tracks near the minimum mass $m_{\rm min}$ which undergoes a blue loop in the instability strip. The metallicity is indicated in the panels and increases from the upper to the lower panel. Masses are indicated along the tracks. Solid lines correspond to the minimum mass, whereas dashed lines correspond to stars which show a reduced blue loop but do not cross the instability strip. The crosses indicate fundamental unstable modes, including the first crossing unstable modes.

$$\log \frac{L}{L_\odot} = 3.21 \log \frac{M}{M_\odot} + 0.51 \qquad \text{for} \qquad Z = 0.02 \qquad (1)$$

$$\log \frac{L}{L_\odot} = 3.23 \log \frac{M}{M_\odot} + 0.54 \qquad \text{for} \qquad Z = 0.01 \qquad (2)$$

---

[2] Above 10 $M_\odot$, the Z=0.004 and Z=0.01 models do not undergo a blue loop. The 12 $M_\odot$ star with Z=0.02 does not undergo a blue loop and reaches a lower L during core He burning than the 11 $M_\odot$ star with the same Z.

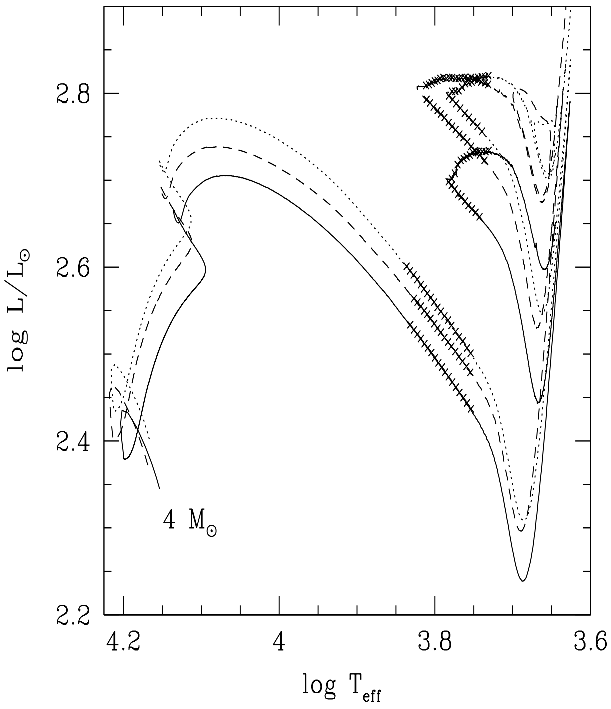

Fig. 2. Evolutionary tracks of 4 $M_\odot$ with different chemical compositions representative of the LMC: $(Z, Y) = (0.01, 0.25)$ (solid curve), $(Z, Y) = (0.008, 0.25)$ (dashed curve) and $(Z, Y) = (0.01, 0.28)$ (dotted curve). The crosses indicate fundamental unstable models.

$$\log\frac{L}{L_\odot} = 3.28\log\frac{M}{M_\odot} + 0.63 \qquad \text{for} \qquad Z = 0.004 \qquad (3)$$

and in the blue loop IS:

$$\log\frac{L}{L_\odot} = 3.55\log\frac{M}{M_\odot} + 0.53 \qquad \text{for} \qquad Z = 0.02 \qquad (4)$$

$$\log\frac{L}{L_\odot} = 3.44\log\frac{M}{M_\odot} + 0.66 \qquad \text{for} \qquad Z = 0.01 \qquad (5)$$

$$\log\frac{L}{L_\odot} = 3.43\log\frac{M}{M_\odot} + 0.85 \qquad \text{for} \qquad Z = 0.004 \qquad (6)$$

Note that the mean luminosity of SMC composition models is brighter than galactic composition models by $\Delta\log L/L_\odot \sim 0.2$. The initial helium abundance affects as well the ML relationship, and an increase of Y from 0.25 to 0.28 for the Z=0.01 sequences yields an increase in $\log L/L_\odot$ by ~ 0.1.

2.2. Evolutionary timescales

The determination of PL relationships and the probability to detect a Cepheid of a given mass in a large sample of data will heavily depend on the time spent in the instability strip. Regarding the first crossing, this time is fixed by the thermal timescale of the star $\tau_{th} = Gm^2/RL \sim 0.8(m/M_\odot)^2 T_{\rm eff}^2 (L_\odot/L)^{3/2}$ yrs. τ_{th} varies typically from $\sim 10^5$ yrs for 3 $M_\odot$ to $\sim 10^4 - 5\,10^3$ yrs for 8-10 $M_\odot$. The time spent in the instability strip during the first crossing is even shorter than τ_{th} and is roughly 100 times shorter than the time spent in the blue loop instability strip.

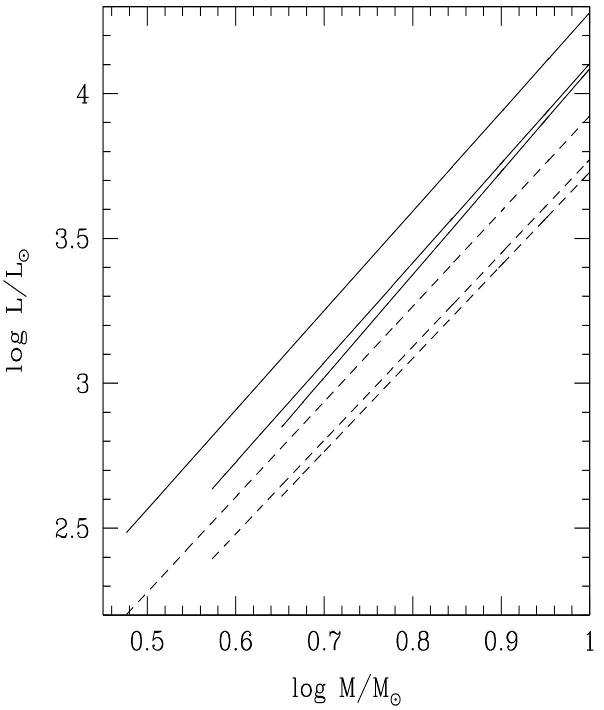

Fig. 3. Mass - Luminosity relationships as a function of chemical composition. The dashed curves correspond to the mean luminosity during the first crossing instability phase and the solid curves correspond to the blue-loop phase. The metallicity decreases from top to bottom and corresponds respectively to: $(Z, Y) = (0.004, 0.25)$ (upper curve), $(Z, Y) = (0.01, 0.25)$ (middle curve) and $(Z, Y) = (0.02, 0.28)$ (lower curve).

Regarding this latter timescale, Fig. 4 displays evolutionary tracks of stars of different masses and indications of the time spent during the core He burning phase. The distribution of the evolutionary timescales in this figure is generic of core helium burning during a blue loop and remains valid independently of metallicity or convection treatment. As shown in Fig. 4, most of the time during core He burning phase is spent near the turnover of the evolutionary tracks. The first branch of the blue loop is characterized by an increase in mass of the He convective core, the expansion of the regions inner to the H burning

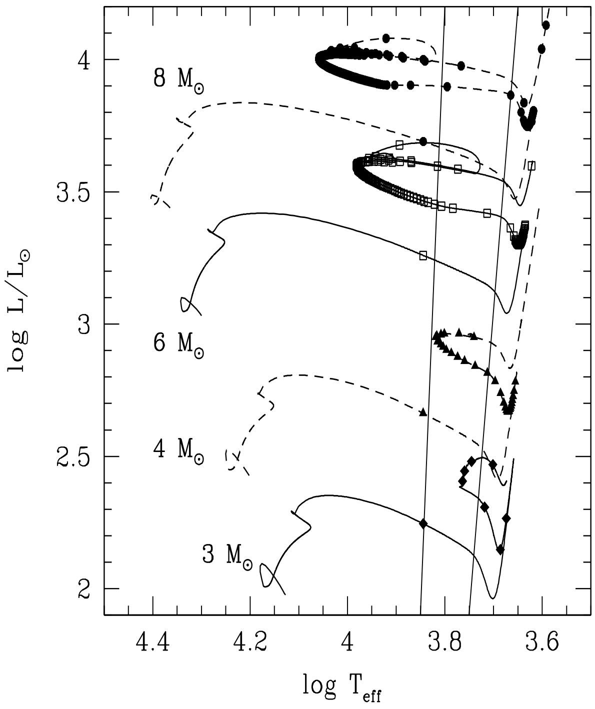

Fig. 4. Evolutionary tracks for stars of different masses, as indicated in the figure, for Z=0.004. Symbols are plotted along each tracks every Δt, with $\Delta t = 10^7$ yrs (full diamonds, 3 $M_\odot$), $\Delta t = 10^6$ yrs (full triangles, 4 $M_\odot$), $\Delta t = 10^5$ yrs (open squares, 6 $M_\odot$) and $\Delta t = 2\,10^4$ yrs (full circles, 8 $M_\odot$). The time count starts on the first crossing at $T_{\rm eff}$ = 7000K. The vertical lines indicate roughly the location of the instability strip.

shell and the contraction of the envelope: evolution proceeds toward higher $T_{\rm eff}$. As the central nuclear fuel (He) is depleted, the central regions start to contract again, resulting in an expansion of the envelope, and the evolution proceeds toward lower $T_{\rm eff}$ on a shorter timescale determined by the faster depletion of He. Interestingly enough, the mean position of a given mass in the IS, taking into account its evolutionary time, is roughly located in the middle of the IS. Thus the time distribution in the IS does not favor a particular position near the IS edges, except for masses near $m_{\rm min}$ for obvious reasons (cf. §3.2 and Fig. 7). This result is valid for all metallicities studied and independently of the convective treatment.

2.3. Uncertainties due to the treatment of convection

In order to estimate the uncertainties of PL relationships relying on stellar evolution calculations, we have analysed the sensitivity of the results to a variation of the mixing length parameter $l_{\rm mix}$ and to the effect of overshooting or any enhanced mixing in the core. The effect of overshooting on stellar models and the necessity to include it or not in order to fit observations has been already widely investigated (see Bressan et al. 1993; El Eid 1994; Pols et al. 1998; and references therein) and is out the scope of the present paper.

An increase of $\alpha_{\rm mix}$ from our standard value 1.5 to 2 results essentially in the well-known shift of the Red Giant Branch to higher $T_{\rm eff}$. However, the ML relationships and the aspect of the blue loops remain essentially unchanged. We will see in §3 that this parameter affects the stability of the models and modifies the width of the IS.

The effect of enhanced mixing in the core as modeled by our simple recipe is more important regarding stellar evolution, and results in an increase of the luminosity for a given mass by 0.15 - 0.20 in log $L/L_\odot$ for our adopted overshoot length $d_{\rm ov} = 0.15 H_{\rm P}$. This is a little less than the mild-overshooting used by Chiosi et al. (1993) with an increase of the luminosity $\log(L/L_\odot)_{\rm ov} = \log(L/L_\odot)_{\rm standard} + 0.25$. The size of the blue loops are affected by overshooting and most importantly the minimum mass $m_{\rm min}$ which undergoes a blue loop increases, in agreement with similar calculations including overshooting (see El Eid 1994 for a detailed discussion).

As discussed in Baraffe et al. (1998), the standard evolutionary models with Z=0.01 do not predict the right position of the faintest Cepheids observed in the EROS-1 and EROS-2 LMC samples, which show an abrupt end of the PL relationship for fundamental mode pulsators at a period P = 2.5 days (Sasselov et al. 1997; Bauer et al. 1998). This observational trend has been confirmed very recently by the MACHO survey (Alcock et al. 1998). Although few objects are observed below this period, the bulk of fundamental mode Cepheids clearly do not extend below this value. One may interpret this abrupt end in terms of the faintest unstable models on a blue loop, since most of the time is spent during this phase. The few objects below 2.5 days may then correspond to first crossing models and their scarcity is representative of the faster evolutionary timescale of this phase (cf. §4).

Our standard calculations for Z=0.01 predict this abrupt end at $P \sim 1.8$ days, corresponding to the blue loop unstable models of $m_{\rm min} = 3.875\ M_\odot$. A possible explanation for this discrepancy is a shortcoming in the stellar evolutionary models which may underestimate $m_{\rm min}$. With our overshooting prescription and an overshoot distance fixed at 0.15 $H_{\rm P}$ the minimum mass $m_{\rm min}$ is shifted to 4.25 $M_\odot$ instead of 3.875 $M_\odot$ for Z=0.01. As shown in §4, this yields better agreement with the lower end of the PL relationship for LMC fundamental mode Cepheids. When applying the same overshooting prescription to Z=0.004 models (*i.e.*, the SMC metallicity), $m_{\rm min}$ is shifted to 3.25 $M_\odot$, instead of 3 $M_\odot$ in the standard case. However, for the SMC, Baraffe et al. (1998) show that the standard models are in excellent agreement with the observed distribution of fundamental mode Cepheids, and overshooting is not required in this case (cf. §4). But the idea of invoking some kind of extra-mixing for LMC evolutionary models but not for the SMC composition in order to improve the comparison with observed fundamental Cepheids is not satisfactory. Our poor understanding of core overshooting in the current stellar evolution theory does not allow any predictions or speculations regarding the efficiency of such mixing as a function of metallicity. We will come back to this problem in §4.

3. Theoretical Period-Luminosity relationships

3.1. Linear stability analysis

In order to get fully consistent calculations between evolutionary and pulsation calculations, a linear non-adiabatic stability analysis is performed directly on the complete evolutionary models along the tracks. This provides fully consistent mass-luminosity-period-evolutionary time relationships and enables us to analyse carefully evolutionary effects on the PL relationships. The pulsation calculations are performed with a radial pulsation code originally developed by Umin Lee (Lee 1985). The main uncertainty inherent to the stability analysis concerns the pulsation-convection coupling, which is presently neglected, *i.e.*, the perturbation $\delta F_{\rm conv}$ of the convective flux is neglected in the linearized energy equation. Such a crude approximation, adopted also in Saio and Gautschy (1998), is resorted to our poor knowledge of the interaction between convection and pulsation, which requires a time-dependent non-local theory of convection. This interaction provides a damping term which is necessary to obtain a red edge for the Cepheid IS. Perturbed models which assume $\delta F_{\rm conv} = 0$ (cf. Fig. 5) remain unstable even near the Red Giant Branch (cf. Saio and Gautschy 1998, Bono et al. 1998a; Yecko et al. 1998).

Several attempts have been made to take into account pulsation-convection coupling in Cepheids with the most recent approach by Yecko et al. (1998; see also Kollath et al. 1998) and BCCM98. A systematic survey of linear properties of Cepheid models including a model of turbulent convection performed by Yecko et al. (1998) shows the extreme sensitivity of the instability strip location on the choice of the several free parameters inherent to the model of convection. As demonstrated by Yecko et al. (1998), the location and width of the IS depend essentially on the three parameters which determine the mixing length, the convective flux and the eddy viscosity. The only possible method to calibrate these parameters is a comparison with observed IS. However, one can expect that a theoretical determination of the IS depends not only on pulsation calculations, but also on stellar evolution properties.

Since the purpose of the present paper is to determine to which extend evolutionary properties are important for the position and width of the IS, we have chosen in a first study to limit the range of free parameters in the pulsation calculations, and to adopt a rather arbitrary criterion for the determination of the IS red edge. A forthcoming paper will be devoted to the uncertainties resulting from the treatment of convection in the pulsation calculations.

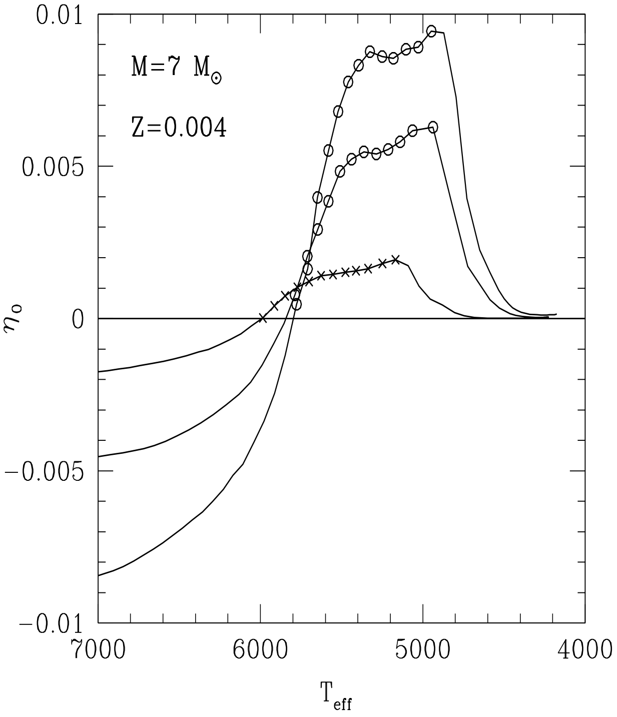

Fig. 5. Evolution of the fundamental mode growth rate η_0 as a function of effective temperature along the evolutionary track of a 7 $M_\odot$ with Z=0.004. The selected unstable modes which define the IS are indicated by crosses on the first crossing and by full circles during the blue loop phase. According to the criterion adopted in the present paper, the red edge is given by the location of the maximum reached by η_0 as $T_{\rm eff}$ decreases.

In the present models, as shown in Fig.5, we assume ad hoc a red line corresponding to the effective temperature where the growth rate reaches a maximum as $T_{\rm eff}$ decreases along the evolutionary track for a given mass. This method is the same as adopted in Chiosi et al. (1993). Adopting a time dependence for the eigenfunctions of the form $\exp(i\sigma_k t)$ where $\sigma_k = \sigma_r + i\sigma_i$ is the eigenfrequency of the k_{th} mode, the growth rate is defined as $\eta_k = -\sigma_i/\sigma_r$. Thus, positive growth rates indicate unstable modes.

3.2. Effect of chemical composition

Since most of the theoretical analysis devoted to Cepheids are based on stability analysis of envelope models and ML relationships independent of metallicity, it is interesting to analyse the uncertainties resulting from such assumptions.

We have tested models by comparing results obtained with the full computations (stellar evolution and pulsation calculations coupled) and with envelope models constructed with constant luminosities. Fig. 6a shows the evolutionary tracks of 7 $M_\odot$ and 11 $M_\odot$ stars with Z=0.004 and Z=0.02 and the fundamental unstable models during core He burning phase. The luminosities adopted for the envelope calculations are derived from our fits given in §2.1 and are indicated by full circles for Z=0.02 (Eq. (4)) and full squares for Z=0.004 (Eq. (6)). The results of the linear stability analysis are shown in Fig. 6b . The differences between the IS location based on the full calculations and envelope models are small when using the metallicity dependent ML relationships. The main differences are due to differences in the luminosity or to departure from the initial composition in the case of full calculations, as a consequence of the first dredge-up. As an example, we note that the red edge given by stability analysis of envelope models for 11 $M_\odot$ with Z=0.02 (full circles) is slightly redder by $\sim$ 100 K than the red edge given by the full calculations (solid curves). This is mostly due to an enrichment of He in the envelope of this star from the initial value Y=0.28 to Y=0.31. When adopting the latter value to construct the envelope models, the red edge is shifted to higher $T_{\rm eff}$, in better agreement with realistic models. However, we note that such evolutionary effects affecting the initial composition are small and yield to a shift of the red edge of at most 100 K in $T_{\rm eff}$. We also stress that this result highly depends on our rather uncertain criterion for the red edge determination.

The most important effect is obtained when adopting for the Z=0.02 models the same ML relationship as derived for Z=0.004 (Eq. (6)). The main result is a shift of the IS toward lower $T_{\rm eff}$ (full triangles) and to a larger width, with a shift of the red edge by 100 to 200 K, compared to the Z=0.004 case (dashed lines and full squares). This example highlights the metallicity dependence of the ML relationship.

The instability strips in period-luminosity and period - $T_{\rm eff}$ diagrams based on our standard models in the core He burning phase are shown Fig. 7 for Z=0.004, 0.01 and 0.02. In agreement with the results of Saio and Gautschy (1998), we do not find significant metallicity effects on the location and width of the IS. We only note that for log $P > 1$, the red edge of the solar metallicity IS moves toward slightly cooler $T_{\rm eff}$. Because of the arbitrariness of our red edge determination and the increasing influence of convection in such models, this result is to be taken with caution. The lower panel of Fig. 7 indicates the mean location in the IS of each mass, taking into account its time spent at a given location in the IS [3]. Except for the particular case of $m_{\rm min}$, indicated by arrows in Fig. 7, the

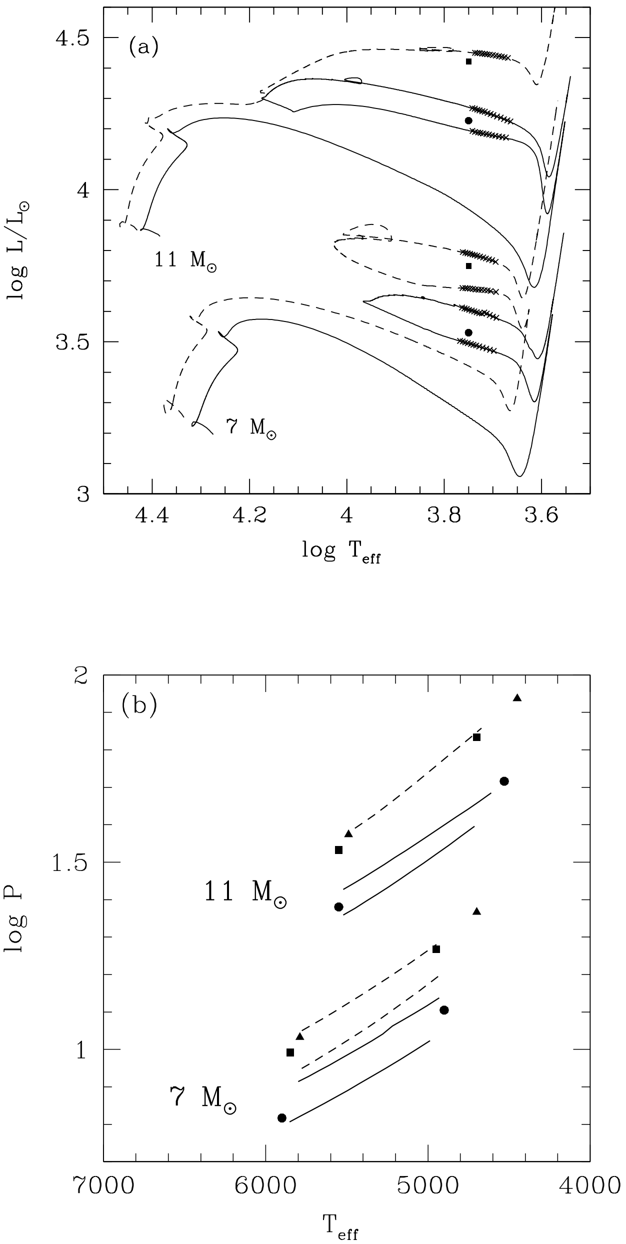

Fig. 6. **(a)** Evolutionary tracks for stars of 7 $M_\odot$ and 11 $M_\odot$, as indicated in the figure, for Z=0.02 (solid curves) and Z=0.004 (dashed curves). The location of fundamental unstable modes during core He burning is indicated by crosses. The full circles indicate the luminosity given by the ML relationship of Eq. (4) for 7 $M_\odot$ and 11 $M_\odot$ and the full squares correspond to Eq. (6). **(b)** Period (in days) of the fundamental mode as a function of $T_{\rm eff}$ for the same models as in (a). The curves correspond to coupled evolutionary and pulsation calculations with same masses and metallicity as in (a). The symbols correspond to the blue and red edges obtained from stability analysis of envelope models with composition (Z,Y) = $(0.02, 0.28)$ and L given by Eq. (4) (full circles) and (Z,Y)=(0.004, 0.25) and L given by Eq. (6) (full squares). The full triangles correspond to (Z,Y)=(0.02, 0.28) envelope models with

mean position given by such weighting function for each stellar mass is roughly located in the middle of the IS, and shows the negligible dependence on Z. Such results do not support the conclusions of Fernie (1990) who find a non uniform population of Cepheids in the IS. The discrepancy between theoretical predictions and such observations has been recently discussed by Gautschy (1999), and is confirmed by the present work. A more detailed analysis is under progress to determine whether the Fernie (1990) results can be explained by an observational bias or by intrinsic properties of stellar models which escape to the present analysis.

---

[3] The mean position is determined from a weighted mean *i.e* for a given model i with age $t(i)$ in the IS, the quantities $L(i)$, $T_{\rm eff}(i)$, etc..., are weighted by the time interval $t(i+1) - t(i)$.

Metallicity however affects the lower end of the period distribution since it modifies $m_{\rm min}$ (cf. Fig. 1). As suggested in Baraffe et al. (1998), the reduction of the He blue loop yields a change of slope in the PL relationship. Because of the metallicity dependence of $m_{\rm min}$, the period at which this change of slope is predicted decreases with metallicity. As illustrated in Fig. 8 for standard models, this change of slope takes place at log $P \sim 0.2$ for Z=0.004, log $P \sim 0.35$ for Z=0.01 and log $P \sim 0.5$ for Z=0.02. Although this value may change due to uncertainties in the convection treatment of the *evolutionary models*, as to be mentioned in the next section, the relative effect due to the metallicity is unaffected by such uncertainties. Fig. 8 displays the unstable modes during the first crossing, which are expected to be observed in a sufficiently large sample of data. As already mentioned, the time spent during this phase is $\sim 1/100$ the time spent in the blue loop. Thus in a large sample of data, one expects to see the trend of a change of slope followed by most of the low period Cepheids, and a few of them with even lower periods which do not show a change of slope and belong to the first crossing. Note that, although the time spent in the first crossing is relatively short, it remains too long to observe any variation of the period on a timescale of years. Indeed, for a 4 $M_\odot$ with LMC composition, we predict a variation of P_0 during the first crossing of less than 10^{-5} days per year.

Finally, we derive PL relationships based on the following method: we assign a mean position to *each* stellar mass, according to the time spent in different locations in the IS, and derive a *linear* least-square fit to these points from $m_{\rm min}$ to 12 $M_\odot$. In the following, all relationships are based on this method, which is more convenient for an analysis of metallicity effects and a comparison with different sample of data over a wide range of periods, than the one adopted by Baraffe et al. (1998), which gives higher weight to the lowest mass stars and favor the low period region.

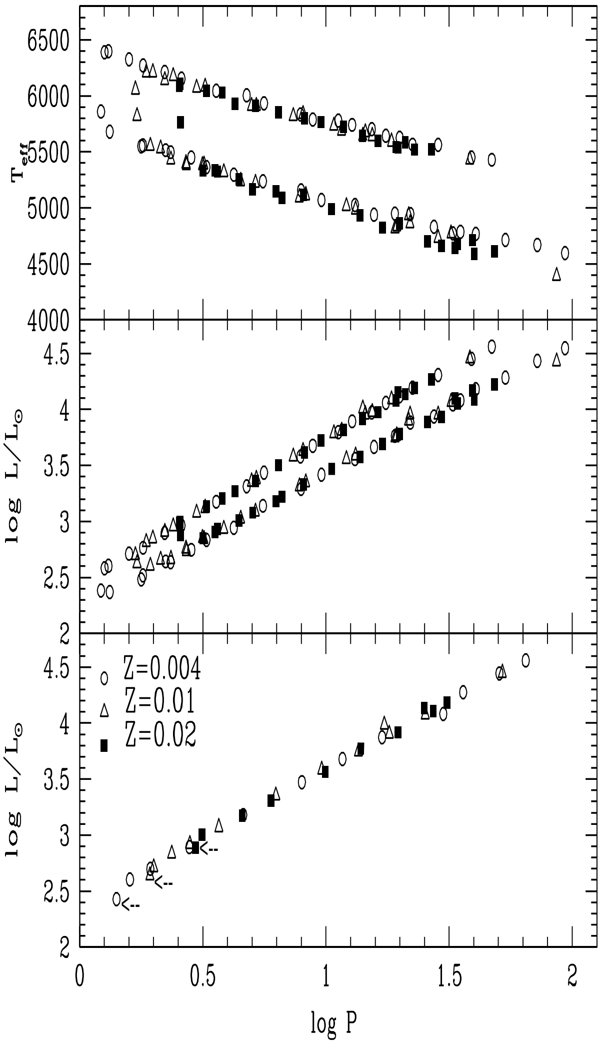

Fig. 7. P - L (middle panel) and P - $T_{\rm eff}$ (upper panel) diagrams for the blue and red edges of the fundamental modes during the core He burning phase of standard models for three metallicities. The lower panel indicates the mean location in the IS of each mass, taking into account the evolutionary times (see text). The arrows indicate the mean position of $m_{\rm min}$ for each metallicity displayed. The symbols correspond to different metallicities (cf. lower panel).

Table 1 summarizes the coefficients of the present PL relationships as a function of metallicity and convection treatment. An inspection of Table 1 shows a negligible dependence of the PL relationships on Z. As expected from Fig. 8, the PL relationships have much steeper slopes near $m_{\rm min}$: we obtain a slope of 1.36 from $m_{\rm min} = 4.75$ $M_\odot$ to 5.5 $M_\odot$ (log $P \lesssim$0.8) for Z=0.02, 1.46 from $m_{\rm min} = 3.875$ $M_\odot$ to 5 $M_\odot$ (log $P \lesssim$0.7) for Z=0.01 and 1.47 from $m_{\rm min}$ = 3 $M_\odot$ to 4 $M_\odot$ (log $P \lesssim$0.6) for Z=0.004. However, PL relationships derived from respectively 5.5, 5 and 4 $M_\odot$ for Z=0.02, 0.01 and 0.004, up to 12 $M_\odot$, yield essentially the same results as obtained in Table 1. This indicates that a unique linear PL relationship is not appropriate on

Table 1. Coefficients of log P – log $L/L_\odot$ relationships (slope, zero-point) for fundamental pulsators as a function of metallicity and convective treatment in the evolutionary models. The standard models refer to $(\alpha_{\rm mix}, d_{\rm ov}) = (1.5, 0)$, *i.e.* $\alpha_{\rm mix} = 1.5$ and no overshooting.

$(\alpha_{\rm mix}, d_{\rm ov})$	(1.5,0)	(2,0)	(1.5,0.15)
Z=0.02	(1.237, 2.347)	-	-
Z=0.01	(1.248, 2.346)	(1.256, 2.386)	(1.270, 2.264)
Z=0.004	(1.239, 2.328)	(1.271, 2.358)	(1.289, 2.265)

the whole range of periods involved in the IS, and that PL relationship based on *low period* Cepheid samples must be taken with caution. Finally, we note that a slight variation of the helium abundance from 0.25 to 0.28 with Z=0.01, or a slight variation of Z from 0.01 to 0.008 with Y=0.25, yields negligible effects on the PL relationships.

Comparison between our blue edges and the one obtained by Saio and Gautschy (1998) shows a *constant* shift of their IS toward brighter L by $\Delta \log L \sim 0.1$ for a given P. This explains the different PL relationships between their work and the present one. Their red edge is determined by shifting the blue edge by $\Delta \log T_{\rm eff} = 0.06$, which differs from the method adopted in the present work, but yields a width of ~ 700 K in agreement with the present work. The reason of the difference of $\Delta \log L \sim 0.1$ is not clear, but is certainly acceptable, since different codes are used. Saio and Gautschy (1998) did not analyze the low mass region where the blue loop extension is reduced, since their analysis is performed for m $\geq 4M_\odot$ for all metallicities. It is worth mentioning that our two independent studies reach the same conclusions regarding the small effects of metallicity on PL relationships.

3.3. Effect of different treatments of convection

In this section we analyse the effect of a variation of $l_{\rm mix}$ and of overshooting on the location of the IS and on the PL relationships. An increase of $l_{\rm mix}$ from 1.5 to 2 in the evolutionary calculations affects essentially the location of the red edge, since the structures of these models are mostly affected by convective transport in their envelope. An increase of $l_{\rm mix}$ yields lower temperature gradients in the region of H and He partial ionization and results in a denser structure for a given T. The net result is a damping effect and a shift of the red edge by $\Delta \log T_{\rm eff} \sim 0.02$ toward hotter $T_{\rm eff}$. However, an inspection of Table 1 shows that the effect on the PL relationships is small.

Overshooting does not significantly modify the location of the IS. As shown in Table 1, overshooting yields slightly different PL relationships compared to the standard case, yielding a maximum of 15% difference in L at a given P. However the effect remains small on the whole range of periods investigated, in agreement with Saio and Gautschy (1998). The previous conclusions regarding the metallicity effects remain valid when overshooting is taken into account.

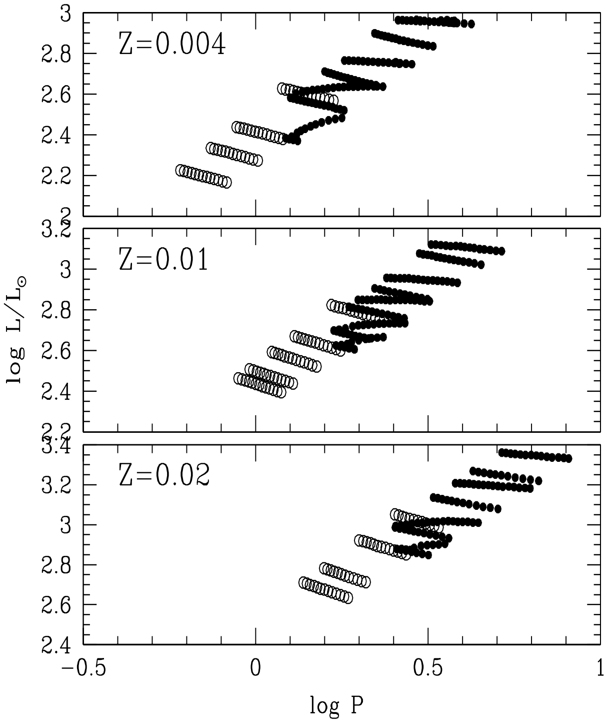

Fig. 8. PL diagram for fundamental modes during the first crossing (open circles) and the blue loop phase (full circles) of standard models as a function of metallicity. The corresponding masses shown in each panel are : 3, 3.25, 3.5 and 4 $M_\odot$ for Z=0.004 (upper panel); 3.875, 4, 4.25, 4.5 and 5 $M_\odot$ for Z=0.01 (middle panel); 4.75, 5, 5.5 and 6 $M_\odot$ for Z=0.02 (lower panel)

As mentioned previously, models including overshooting predict a change of slope at the lower end of the PL relationship at *higher* P, compared to the standard case. As shown in Fig.9, this change of slope is expected at log $P \sim 0.5$ for Z=0.004 and log $P \sim = 0.65$ for Z=0.01. As for the standard models, derivation of PL relationships on a mass range near $m_{\rm min}$ yields much steeper slopes as well.

3.4. First overtone pulsators

The main effects of chemical composition and convection treatment on the PL relationships remain the same for first overtone pulsators. We thus do not find significant effect of Z on the location of the 1H IS and the PL relationships. Table 2 summarizes the PL relationship coefficients as a function of metallicity for the standard models.

The minimum mass $m_{\rm min}$ undergoing a blue loop in the *fundamental mode* IS does not fulfill the instability

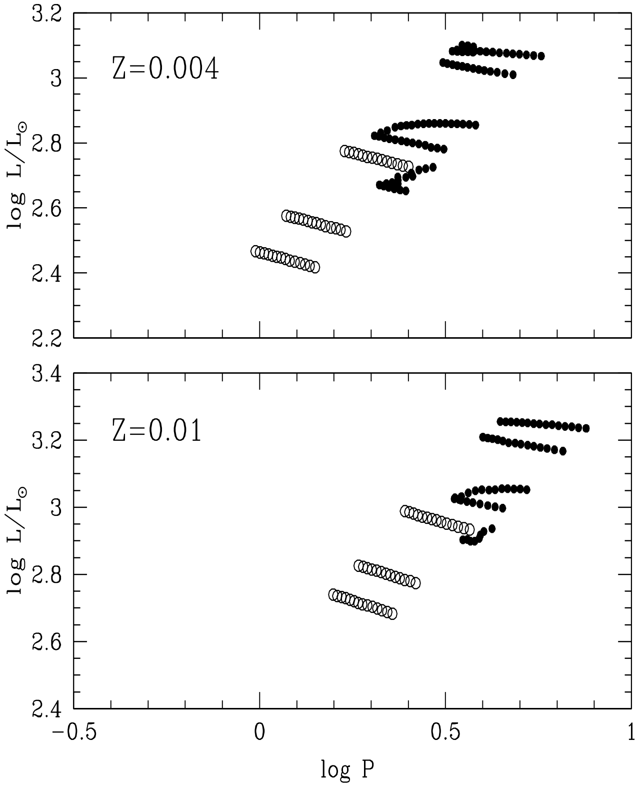

Fig. 9. Same as Fig. 8 for models including overshooting with $d_{\rm ov} = 0.15$. The corresponding masses shown in each panel are: 3.25, 3.5 and 4 $M_\odot$ for Z=0.004 (upper panel); 4.25, 4.5 and 5 $M_\odot$ for Z=0.01 (lower panel).

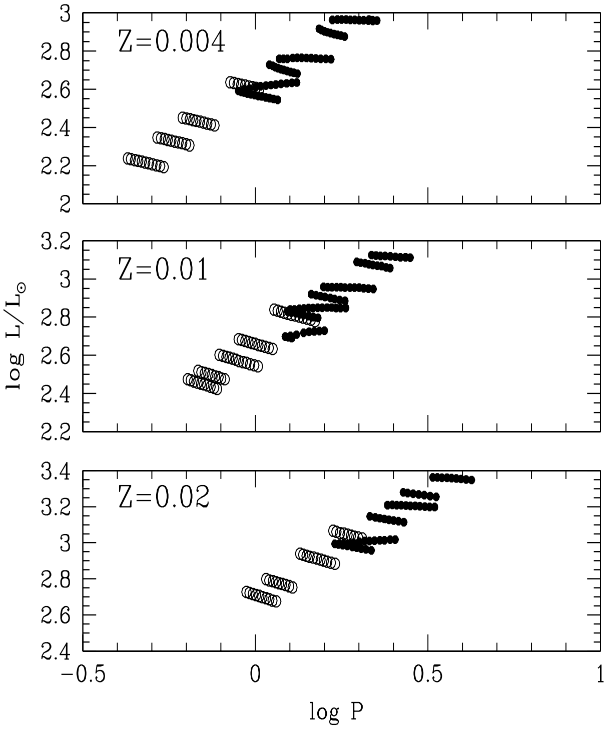

Fig. 10. Same as Fig. 8 for first overtone pulsators. For the first crossing phase, the same masses as in Fig. 8 are displayed. For the blue loop phase, the minimum masses displayed are $m_{\rm min} = 3.25\ M_\odot$ for Z=0.004, $m_{\rm min} = 4 M_\odot$ for Z=0.01 and $m_{\rm min} = 5 M_\odot$ for Z=0.02.

Table 2. Same as Tab. 1 for first overtone pulsators and standard models.

$(\alpha_{\rm mix}, d_{\rm ov})$	(1.5,0)
Z=0.02	(1.245, 2.661)
Z=0.01	(1.281, 2.618)
Z=0.004	(1.258, 2.611)

criterion for 1H, because of its hotter $T_{\rm eff}$ compared to F IS. Thus, $m_{\rm min}$ increases for 1H and corresponds to 3.25 $M_\odot$ for Z=0.004, 4 $M_\odot$ for Z=0.01 and 5 $M_\odot$ for Z=0.02. We predict as well the feature of a change of slope at the lower end of the PL relationship, as shown in Fig. 10. However the effect seems to be less pronounced, because of the significant reduction of the IS width, by more than 400K, compared to F modes. We are aware that this result strongly depends on our adopted criterion to determine the red edge, which fixes the width of the IS. This point is further analysed on the basis of comparisons with observations in §4.

4. Comparison with observations

4.1. Synthetic spectra

In order to perform comparisons with observed magnitudes and colors, we have used version 10.3 of the model atmosphere code `PHOENIX` to calculate a set of static atmosphere models, and their synthetic spectra, in local thermodynamic equilibrium (LTE), using a spherically symmetric radiative transfer. The atomic and molecular opacities are included in a direct line-by-line opacity sampling treatment (i.e. no pre-tabulation) with a line selection criterion applied at each model iteration and based on the strength of the line relative to the strength of local continuum opacities. Further details of the general input physics are discussed in Hauschildt et al. (1998) and references therein. The model grid englobes the parameter range of Cepheids, *i.e.*, $T_{\rm eff} = 4000 - 7000K$ and $\log g = 0 - 3.5$, and is an extension to lower gravity of the models recently developed by Hauschildt et al. (1998), which successfully describe M-dwarf atmospheres (cf. Allard et al. 1997). Convective mixing is included according to the Mixing Length Theory (MLT). Only models with a mixing length of unity and a sphericity corresponding to a stellar mass of $M = 5\,M_\odot$ were calculated. We have checked that for the range of $T_{\rm eff}$ and gravities involved in the present study, the sensitivity of the synthetic spectra to the stellar mass is small, justifying the above approximation. Only for low gravity and effective temperature, the effect can be important and reaches 10% difference in models with $T_{\rm eff} = 3600\,{\rm K}$, log $g = 0.0$ and solar abundances. For higher gravities, this effect vanishes, as expected. The depth-independent microturbulence used in the model atmosphere calculations is 2 km/s. Changes will affect high-resolution spectra far more than the broad band colors used here, so we have not considered other values of the microturbulence.

In the following, the $BVRI$ magnitudes are based on the Johnson-Cousins system (Bessell 1990), whereas the JHK magnitudes are defined in the CIT system (Leggett 1992). Since some of the observations used in the present paper are based on the SAAO-Carter system, we have also calculated magnitudes in this system, using the filter transmission curves kindly provided by P. Fouqué. The J-band is mainly affected by the choice of the photometrical system, whereas the K-fluxes in both systems do not differ by more than 0.05 mag. Comparison between our results in CIT and Carter systems yields the following conversion equation:

$$(J-K)_{\rm CIT} = 0.91\,(J-K)_{\rm Carter}, \tag{7}$$

adopting $K_{\rm CIT} = K_{\rm Carter}$. This equation, which is accurate within less than 0.01 mag for the range of $T_{\rm eff}$ and surface gravity of interest, is used in the following to transform in the CIT system observations given in the Carter system. We stress that Eq. (7) is *only valid for giants* but fails for cooler and higher gravity objects.

4.2. Period - Magnitude relationships

This section is devoted to comparison with observations in period - magnitude diagrams. The metallicity effects on the period - magnitude relationships are analyzed and quantified in §5.

4.2.1. Galactic Cepheids

The solar metallicity models are compared to the sample of galactic Cepheids of Gieren et al. (1998, GFG98). The careful selection of stars in this sample and the determination with good accuracy of their radius and distance yield lower dispersions of the derived period-magnitude relationships and thus provide an excellent test for theoretical models. Comparison between models and observations are shown in Fig. 11 in the V, J and K bandpasses. The J-magnitudes of GFG98 are given in the Carter System, and have been transformed in the CIT system according to (7).

In a similar way as done for the PL relationships in §3, we derive period - magnitude relationships. The coefficients of these relationships are given in Tab. 3 for each Z studied. Fig. 11 shows a comparison between the predicted relationships and those derived by GFG98 using both galactic and LMC Cepheids.

Excellent agreement is found between models and data in the three bandpasses, as well as between the theoretical and observed mean PL relationships. The present models provide a much better match to observations than the BCCM98 models, based on non-linear calculations but not on consistent evolution-pulsation calculations, and compared to the same data by GFG98. For galactic Cepheids with log $P > 1.3$, a better agreement in a $P - M_{\rm V}$ diagram is reached with the Z=0.008 models of BCCM98, whereas the Z=0.02 models clearly depart from the observed trend. The reason invoked for such discrepancy is the possible spread in metallicity of galactic Cepheids, as recently shown by Fry and Carney (1997). However, the analysis of BCCM98 implies that most of the long period Cepheids observed are sub-metallic. We note that two of the GFG98 Cepheids, T Mon (log $P = 1.43$) and SV Vul (log $P = 1.65$), are metal-rich with [Fe/H] = 0.09 and [Fe/H]=0.06 respectively, according to Fry and Carney (1997). Moreover, if one assumes that the Galactocentric distance $R_{\rm gal}$ is a crude indicator of metallicity (cf. GFG98), since the galactocentric distance of Cepheids with log $P > 1.3$ in the sample of GFG98 is not systematically greater than $R_{\rm gal}(\odot)$ (cf. Gieren et al. 1993), there is no reason to suspect that all these Cepheids have subsolar metallicities (Fouqué, priv. com.). These arguments seem to exclude a possible selection effect in favor of the detection of long period sub-metallic Cepheids and weaken the argument of BCCM98.

4.2.2. LMC Cepheids

Fig. 12 shows the comparison between the present standard models and observations in period - magnitude diagrams for the LMC. The data in the V-band are taken from GFG98, based on the sample of Tanvir (1997), from Laney and Stobie (1994, LS94) and from the EROS1 sample (Sasselov et al. 1997). The magnitudes provided by GFG98 and LS94 are already dereddened. The EROS $(B_{\rm E}, R_{\rm E})$ magnitudes are transformed in the Johnson V magnitude according to Beaulieu et al. (1995), and for the reddening correction, we adopt $E(B-V)$=0.10 and $R_{\rm V}$ = 3.3, as in Baraffe et al. (1998). For the J- and K- bands, the data of GFG98 are used and transformed in the CIT photometrical system. The distance modulus adopted in Fig. 12 is 18.50.

The same excellent agreement is found between models and data in *all* bandpasses. Models with overshooting or with $l_{\rm mix} = 2$ yield slightly different PL relationships (§. 3.3), but we stress that it is impossible to discriminate between standard models and models including overshooting when comparing to bare data in period - magnitude diagrams. Thus, comparison of theoretical and observed period - magnitude diagrams and relationships cannot be used to determine the amount of extra-mixing or the mixing length parameter required in evolutionary models.

A clear distinction between our standard models and models with overshooting is however possible in terms of the minimum period observed. As mentioned previously (cf. §2.3) and in Baraffe et al. (1998), standard models for Z=0.01 predict fundamental pulsators during the blue loop phase down to $\log P = 0.25$ (cf. Fig. 8), in contradiction with the observed end of the EROS and MACHO PL distribution at $\log P \sim 0.4$. Standard models with Z=0.008 predict even lower period for the end of the distribution, since $m_{\rm min}$ decreases. A slight increase of Y from 0.25 to 0.28 for the standard models with Z=0.01 slightly increases this period up to $\log P \sim 0.3$, since it yields slightly brighter models and the same $m_{\rm min}$ (cf. §2.1 and Fig. 2). But this does not solve the problem. Only models including overshooting can yield better agreement, since they predict higher $m_{\rm min}$ (cf. Fig. 9). This problem is further discussed with the analysis of period histograms in §4.5.

4.2.3. SMC Cepheids

Comparison between SMC data and the present standard models for Z=0.004 is shown in Fig. 13. Observations are from LS94, which are already dereddened, and from Sasselov et al. (1997) with an extinction coefficient $E(B-V)$=0.125 and $R_{\rm V} = 3.3$, as adopted in Baraffe et al. (1998). We adopt the distance modulus $(m-M)_0 = 18.94$ of LS94. Note that the SMC Cepheids observed by EROS are in the main bar and the far arm of the SMC and are not likely to belong to the centroid of the SMC (Beaulieu, priv. com.), resulting in a larger distance modulus difference with the LMC by about 0.15 mag compared to other studies (Caldwell & Coulson 1986; LS94). We however adopt the same distance modulus for both EROS and LS94 data for sake of simplicity.

The same agreement is reached as previously between data and models in Fig. 13, as well as between the predicted period - magnitude relationships and the observed one, although the GFG98 relationships are based on galactic and LMC Cepheids. This already illustrates the small metallicity effect predicted by the models on period - magnitude relationships, as analysed in §5.

Regarding the observed minimum period, Baraffe et al. (1998) have analysed this point in detail , with the same EROS data. In this case, the standard models do a better job and predict the correct position of the faintest Cepheid observed (cf. Baraffe et al. 1998 and §2.3). The overshooting models predict a minimum period $\log P = 0.3$ for models undergoing a blue loop, which is excluded by observations (cf. Fig. 13 and Bauer et al. 1998). As for the LMC composition, and except for the determination of this minimum period, period - magnitude diagrams and relationships cannot be used to discriminate standard models from models with overshooting.

Our explanation by an evolutionary scenario of the observed change of slope near $P = 2$ days for fundamental pulsators (cf. Baraffe et al. 1998) has been questioned by Bauer et al. (1998), arguing that such a change of slope should also be observed for 1H Cepheids. According to Bauer et al. (1998), this change of slope is not apparent. However, as mentioned in §3.4, this feature is expected to be less pronounced for 1H than for fundamental pulsators (cf. Fig. 10). Although this could provide a nice explanation for the observed Cepheids in the SMC, we remain extremely cautious with such interpretation however, since we note several discrepancies between observed and predicted 1H pulsators. Fig.14 shows the comparison of 1H pulsators with our standard models for Z=0.004 and Z=0.01 and the EROS SMC and LMC data (Sasselov et al. 1997) respectively. For Z=0.004, the models predict that 1H pulsators with $\log P \lesssim 0$ belong to the first crossing phase, which concerns $\sim 1/10$ of the observed 1H pulsators. This is statistically difficult to explain since comparison between the time-scales during the first crossing and the blue loop phases predicts less than 1/100 of 1H pulsators in the first crossing. Regarding now the end of the distribution at high P, models predict unstable 1H modes up to $\log P \sim 1$, whereas 1H Cepheids are not observed above $\log P \sim 0.5$, corresponding to $\sim 5M_\odot$ for the Z=0.004 standard models. One possible explanation for such discrepancies is to suppose that models in the first crossing phase, although unstable in both F and 1H modes according to linear stability analysis, favor 1H as the dominant mode. Similar reasons can be invoked for $m \gtrsim 5M_\odot$, for which this time F modes become the dominant mode. Only non-linear calculations can test this scenario. Note that if indeed first crossing models are preferably oscillating in 1H mode, the higher number of this type of pulsators near $m_{\rm min}$ provides an other explanation for the non detection of the change of slope near $m_{\rm min}$, since first crossing models do not show any change of slope (cf. §3.4 and Fig. 10).

The other possible reason is a shortcoming due to our neglect of the convection-pulsation coupling, yielding an erroneous IS. We indeed note that the models do not reach the blue edge of the IS, for both the SMC and the LMC (cf. Fig. 14). Models with overshooting or with $l_{\rm mix} = 2$ do not yield better agreement. Only a decrease of the distance modulus of the SMC and the LMC by 0.3 mag can bring the predicted and observed location of the 1H IS in agreement. However, with such smaller distance moduli for both Clouds, the models do not reproduce anymore the observed F pulsators in period - magnitude diagrams. Since more data are available for F pulsators, the models can be better tested against these observations, and we rather believe distance moduli based on F pulsators. Moreover, we note that according to Yecko et al. (1998), the 1H IS seems to be more sensitive to variations of parameters involved in the convection-pulsation coupling model than the F IS. This point suggests that the

Table 3. Coefficients of the log P - Magnitude relationships (slope, zero-point) for fundamental pulsators as a function of metallicity for standard models.

	M_V	M_I	M_J	M_K
Z=0.02	(-2.905, -1.183)	(-3.102, -1.805)	(-3.256, -2.183)	(-3.367, -2.445)
Z=0.01	(-2.951, -1.153)	(-3.140, -1.769)	(-3.286, -2.157)	(-3.395, -2.428)
Z=0.004	(-2.939, -1.081)	(-3.124, -1.686)	(-3.262, -2.076)	(-3.369, -2.350)

neglect of the pulsation-convection coupling in the present linear stability analysis affects 1H modes more and yields an inaccurate IS, whereas fundamental modes are less sensitive to such approximation, a suggestion supported by the general good agreement reached with F Cepheid observations. This problem will be addressed in more details in a forthcoming paper by analysing the uncertainties of the convective treatment in the *pulsation* calculations. Period - magnitude relationships for 1H will be given in this forthcoming work.

4.3. Period - Color relationships

In this section, models are compared to galactic, LMC and SMC Cepheids in period - color diagrams. As expected from the previous results, the uncertainties due to convection treatment in stellar models hardly affect the location of the IS in such diagrams. We thus concentrate our analysis on standard models.

Fig. 15 shows the comparison of galactic Cepheids with the Z=0.02 models, Fig. 16 corresponds to Z=0.01 models and LMC Cepheids and Fig. 17 to Z=0.004 models and SMC Cepheids. The PC relationships (solid curves) derived from our models are displayed in each figures for the corresponding metallicity. The coefficients are given in Tab. 4. The PC relationships derived by LS94, based on the sample with reasonably complete $BVJHK$ light curves, is shown in figures 15-17. These observed PC relationships take into account the zero-point (ZP) shifts of LS94 for the Magellanic Clouds. First, we note the general good agreement for $(B-V)$ and $(V-K)$ colors for the three metallicities displayed, although the predicted colors seem to be too red compared to observations for log $P \lesssim 1$. This trend is more pronounced for the SMC data (cf. Fig. 17). Regarding $(J-K)$ colors, the models are bluer than observations by $\sim 0.05-0.1$ mag, this trend being more pronounced for galactic and LMC data (cf. Fig. 15-16). We note as well that the positions of objects in the theoretical IS are fully consistent for $(B-V)$ and $(V-K)$ colors, whereas the same objects appear at a different location in the IS in the P - $(J-K)$ diagram. This discrepancy appears also for SMC data (cf. Fig. 17), although the models reproduce satisfactorily the data in $(J-K)$. The possible sources of such discrepancies are analysed in §5.

Table 4. Coefficients of the log P - color relationships (slope, zero-point) for fundamental pulsators as a function of metallicity for standard models.

	$B-V$	$J-K$	$V-K$
Z=0.02	(0.246, 0.535)	(0.110, 0.261)	(0.462, 1.262)
Z=0.01	(0.239, 0.497)	(0.108, 0.271)	(0.443, 1.275)
Z=0.004	(0.231, 0.448)	(0.106, 0.274)	(0.429, 1.268)

The present models give a better match to observations than the Chiosi et al. (1993) models, which predict bluer $(B-V)$ colors for the LMC and SMC Cepheids, and the BCCM98 models, which predict significantly redder $(B-V)$ and $(V-K)$ colors for galactic Cepheids. These two previous studies seem to overestimate the metallicity effect on colors. Chiosi et al. (1993) attribute this discrepancy to the $(B-V$, log $T_{\rm eff})$ relations used in their analysis. In the case of BCCM98, the discrepancies stem more likely from the large metallicity effect they find on the location of the IS, since an increase of Z results in a significant shift of their IS toward cooler $T_{\rm eff}$. Whereas their models reach good agreement in period - magnitude and period-color diagrams with the SMC data, slight discrepancies appear already for the LMC data and become larger in both diagrams for galactic Cepheids. The large metallicity effect found by BCCM98 is then questionable. The metallicity effects found on the present period - color relationships are analysed and quantified in §5.

4.4. Period - radius relationships

Comparison between models and observations of GFG98 and Bersier et al. (1997) in a period - radius (PR) diagram is performed in Fig. 18 for F and 1H pulsators. The general agreement for F pulsators is good, although the models slightly overestimate the radius for log $P<1$. The comparison of the observed (solid line) and predicted PR relationships (dashed line) illustrates better this discrepancy. For 1H pulsators, the observed sample is unfortunately too small to test the models. Interestingly enough, we note that the dispersion due to the width of the IS for both F and 1H pulsators is almost parallel to the relationship, resulting in a small intrinsic dispersion due to the IS itself. The coefficients of the PR relationships as a function of Z and convective treatment are given for fundamental pulsators in Tab. 5.

We find a small effect due to metallicity on the PR relationship, with a maximum effect of 7% on R at a given

Table 5. Coefficients of the log $P-\log R/R_\odot$ relationship (slope, zero-point) for fundamental pulsators as a function of metallicity and convective treatment in the evolutionary models.

$(\alpha_{\rm mix}, d_{\rm ov})$	(1.5,0)	(1.5,0.15)
Z=0.02	(0.714, 1.143)	-
Z=0.01	(0.717, 1.142)	(0.713, 1.123)
Z=0.004	(0.709, 1.129)	(0.734, 1.096)

P. We find as well small effects due to uncertainties of convection treatment in the stellar models: models with overshooting or with $l_{\rm mix}$=2 yield essentially the same PR relationships, with a maximum effect of 7% on R at a given P. Note that the effect of uncertainties due to convection in the stellar models is of the same order as the effect of Z. We therefore hardly expect this metallicity effect to be observable.

For 1H pulsators, the PR relationships for the Z=0.02 models shown in Fig. 18 is:

$$\log \frac{R}{R_\odot} = 0.723 \log P + 1.266. \tag{8}$$

The effect of Z on the 1H PR relationship is the same as for fundamental pulsators.

Our results are rather similar to those of Bono et al. (1998b), although they mention up to 9% variation of the radius due to metallicity effect. They find the same discrepancy between models and the lowest period Cepheids as mentioned above. We urgently need more observational data in order to determine whether this discrepancy stems from shortcomings in the method used to determine R for low period Cepheids (see Bono et al. (1998b) for discussion) or from shortcomings in the models.

4.5. Period-histograms

The coupling between evolutionary and pulsation calculations provides the opportunity to construct period-histograms, taking into account a MF and evolutionary timescales, as done for the statistical PL relationships derived in Baraffe et al. (1998). Since histograms give the number of Cepheids in a bin of period and are independent of photometrical, reddening or distance uncertainties, they provide an interesting observational constraint. The effect of evolutionary times dominates that of the MF. In the following, a Salpeter MF is adopted with an exponent -2.35. We have checked that a variation of the MF slope from -2 to -4 does not alter the position of the main peak and yields less than 8% effect on the number of objects in a period-bin.

For the SMC (cf. Fig. 19a), the models are compared to the period-histogram provided by the EROS-1 collaboration (Sasselov et al. 1997). The general shape predicted by the standard models is in good agreement with observations. The bulk of observed Cepheids at log $P \sim 0.1-0.3$ is correctly reproduced by the models and corresponds to models undergoing a blue loop near $m_{\rm min} = 3\ M_\odot$ (cf. Fig. 8). We note however that our calculations overestimate the number of these short-period Cepheids. A similar distribution is obtained for models with a different $l_{\rm mix}$. As expected, the histogram excludes calculations performed with overshooting, which shifts the main peak to higher periods by $\Delta \log P \simeq 0.2$.

For LMC Cepheids (cf. Fig. 19b), models are compared to the fundamental period-frequency distribution provided recently by Alcock et al. (1998). The standard models do not explain the observed histogram, as expected from the discrepancy regarding the observed minimum period (cf. §4.2.2). In this case, the theoretical histogram (dashed line) exhibits a peak around $\log P \sim 0.3$, instead of the observed peak around $\log P \sim 0.5$ in the MACHO sample. Models including overshooting could shift the peak toward the observed one. We note that at the time the present calculations with overshooting were performed, the only available sample was the EROS-1 LMC sample of data, which shows a peak at log $P \sim 0.6$. This motivated our choice of the overshooting length $d_{\rm ov} = 0.15 H_{\rm P}$. The main peak of the MACHO LMC sample appears however at shorter periods than the EROS data. In this case, a smaller $d_{\rm ov}$ than presently adopted can provide better agreement with observations. The detailed understanding of the observed period-histogram of LMC Cepheids has been already analyzed by Alcock et al. (1998). They note also difficulties to reproduce the observations, invoking a non constant star formation rate to explain the long period tail after the maximum and anomalous Cepheids resulting from binary coalescence to explain the short-period Cepheids ($\log P \lesssim 0.4$). One of the arguments given in Alcock et al. (1998) in favor of such an exotic population of Cepheids concerns the double-mode Cepheids, which according to Morgan and Welch (1997) can only be explained by non-standard ML relationships. However, Baraffe et al. (1998) have shown that these double-mode Cepheids can be explained naturally by first crossing models. Such a suggestion is supported by statistical arguments (cf. Baraffe et al. 1998). The presence of short-period Cepheids below the main peak could therefore be explained by first crossing models. Our main concern is thus not the presence of these short-period Cepheids, contrarily to Alcock et al. (1998), but rather the failure of standard models to reproduce the main peak of the LMC distribution, although they provide a good fit to the SMC distribution (cf. Fig. 19a). This problem deserves further analysis and definitely requires the confirmation of the minimum periods observed in the MC's by similar surveys.

Finally, predictions for galactic models are displayed in Fig. 19c. The main peak is located at log $P \sim 0.5$ for standard models, with a sharp break at log $P \sim 0.4$ (cf. Fig.8).

5. Discussion

The general agreement obtained between present calculations and observations in period - magnitude, -color and -radius diagrams gives us some confidence about the analysis of metallicity effects based on the present models. We will first concentrate on period - magnitude relationships. The effect of metallicity is more pronounced in the B bandpass in the range of interest $T_{\rm eff} = 6500{\rm K} - 4400$ K, due to the dominant metallic line absorption, and it decreases at longer wavelengths. For given gravity and $T_{\rm eff}$ in the above-mentioned range, a decrease of metallicity from Z=0.02 to Z=0.004 yields a maximum increase by ~ 0.1 mag of the B-flux, and consequently a decrease of the fluxes redward, of less than 0.05 mag in the V- and I-bandpasses, 0.03 mag in J and 0.02 mag in K.

An inspection of the period - magnitude relationships given in Tab. 3 show rather small effects of Z. A variation of Z from 0.02 to 0.004 yields a difference in magnitude at a given P of less than 0.12 mag in $VIJK$ bandpasses between log $P = 0.5 - 2$. Same quantitative effects of Z are found with overshooting models.

The comparison between predicted and observed (cf. GFG98) PL relationships shows different slopes and zero-points, although the data are well bracketed by the models (cf. Fig. 11-13). The resulting differences in magnitudes between our relationships and those of GFG98, for a given P, are however small, and amount to less than 0.15 mag in V, 0.25 mag in I, 0.35 mag in J and 0.25 mag in K. We note that these maximum discrepancies appear for the highest periods observed. The largest discrepancy between observed and predicted relationships appear in the J-band, although it can be reduced by ~ 0.1 mag by deriving a $P - M_{\rm J}$ relationship in the Carter system. The models however seem to predict systematic higher J-fluxes, and to a lesser extend I-fluxes, than GFG98 for a given P.

The present effect of metallicity on the $P - M_V$ relationship is of the same order as found by Chiosi et al. (1993), but their relationships differ significantly from the present one and that of GFG98 by more than 0.2 mag at log $P > 1$, up to ~ 0.5 mag at log $P = 2$. As already mentioned, the present results significantly differ from the results of BCCM98, who mention large metallicity effects, up to $\delta M_{\rm V} \sim 0.77$ and $\delta M_K \sim 0.42$ between the galactic and the SMC Cepheids. We note that their $P - M_{\rm V}$ relationship for galactic Cepheids yield discrepancies with the observed relationship of GFG98 of ~ 0.4 mag for log $P > 1$ up to ~ 1 mag at log $P \sim 2$. As already mentioned, the possible contamination of the sample by submetallic galactic Cepheids cannot be entirely responsible for such important discrepancies. The models of BCCM98 are based on non-linear calculations accounting for the coupling between pulsation and convection. According to the systematic analysis of Yecko et al. (1998), the recipes used nowadays to describe the convection-pulsation coupling still require a certain number of free parameters, which can significantly affect the location of the IS. In the work of BCCM98, the sensitivity of the results to such uncertainties is not clear, and should certainly be analysed. Moreover, as shown in §3.2 and Fig. 6, adopting the same ML relationship for different Z, as done in BCCM98, favors a shift of the IS location toward cooler $T_{\rm eff}$ as Z increases. However, this effect cannot explain alone the large shift found by BCCM98.

Regarding now PC relationships, the effects of metallicity are more detectable, above all in $(B - V)$, as shown by models and observations in Fig. 15-17. The comparison between the relationships given in Tab. 4 shows that as Z decreases from 0.02 to 0.004, $(B - V)$ gets bluer at a given P by $\sim 0.1 - 0.12$ mag. A comparison of the blue and red edges of the IS between Z=0.02 and Z=0.004 shows the same shift for both edges toward the blue as Z decreases, which reflects essentially the intrinsic effect of metallicity on this color. Similar effect is found by LS94, although slightly larger, since LS94 mention a zero-point (ZP) shift between galactic and SMC Cepheids of 0.215 mag.

For the $(J - K)$ colors, a variation of Z from 0.02 to 0.004 yields less than 0.01 mag effect at a given P, which is consistent with the corresponding 0.033 mag effect quoted by LS94. However, the models seem to predict $(J - K)$ (and $(H - K)$) colors systematically bluer than observations by $\sim 0.05 - 0.1$ mag. The slight discrepancy mentioned previously for $M_{\rm J}$, and the different positions of objects in the theoretical IS predicted by $(J - K)$ colors compared to $(B - V)$ or $(V - K)$ colors (cf. §4) suggest a possible overestimate of the fluxes in the IJH bands.

Finally, for (V-K) colors, the effect of metallicity is smaller than 0.06 mag over the whole range of P explored. LS94 quotes a larger effect of Z on this PC relationship, with a shift of the ZP from galactic to SMC Cepheids of 0.153. BCCM98 find an extremely large effect, up to 0.65 mag at log $P = 2$, due to the shift of the IS toward cooler $T_{\rm eff}$ as Z increases. However, for *galactic Cepheids*, the BCCM98 PC relationships differ by more than 0.2 mag compared to the LS94 relationship for log $P > 1$, whereas we find no more than 0.1 mag difference for the same range of period. For the SMC composition, the $P - (V - K)$ relationship given by BCCM98 yields more than 0.2 mag difference in color compared to the relation given by LS94, for log $P > 1$, whereas our results do not differ by more than 0.2 mag.

Regarding the uncertainties of the present atmosphere models, we have neglected the effects of departures from local thermodynamic equilibrium, departures from hydrostatic equilibrium on the atmospheric structure, and the effects of varying the mixing length parameter. Since NLTE effects are affecting the atomic line formation, we expect these to mainly affect the synthetic spectra in the ultraviolet to visual spectral range (U, B, and V bandpasses) where atomic transitions dominate the spectral distribution of these stars. The propagation of hydrodynamic chocs in the atmospheres may also affect the synthetic spectra by modifying the thermal structure of the atmosphere. It is difficult to estimate these effects at this point, but observation of such effects in cooler Mira variable stars suggest a pronounced modification of the spectra due to choc propagation in the near-infrared bandpasses (J, H and K). Convection, on the other hand, is limited to the lowermost regions of the atmospheres ($\tau > 15$), and the synthetic spectra are insensitive to changes of the mixing length parameter. All the possibilities mentioned above could be the source of the observed color discrepancies quoted previously and remain to be explored in subsequent works.

6. Conclusion

We have performed consistent stellar evolution and pulsation calculations in order to determine evolutionary effects on the properties of Cepheids as a function of metallicity. We have investigated a range of metallicities representative of the Galaxy and the MC populations. The calculation of atmosphere models and synthetic spectra in the present work allows accurate comparisons with observations. We find *unprecedented* levels of agreement with the most recent observations of Cepheids in the Galaxy and the MC's in period - magnitude *and* period - color diagrams. The good agreement with different observational constraints adds credibility to the present models and to the conclusions regarding the metallicity effects. Our main results can be summarized as follow:

- A change of slope in the PL relationships is predicted near the minimum mass $m_{\rm min}$ which undergoes a blue loop in the instability strip during core He burning. The critical period at which this change of slope occurs decreases with Z. For standard models, it takes place at log $P \sim 0.2$ for Z=0.004, log $P \sim 0.35$ for Z=0.01 and log $P \sim 0.5$ for Z=0.02. These values are affected by uncertainties due to convection treatment in the stellar models, and increase when overshooting is taken into account. However, the above mentioned Z dependence is not affected by these uncertainties.
- Taking into account the time spent in the IS for each mass, the mean position is roughly in the middle of the IS, except for masses near $m_{\rm min}$. This indicates that evolutionary timescales do not favor any particular position near the edges, in contradiction with the finding of Fernie (1990). This result is independent of the convective treatment used in the stellar models. A linear least-square fit to the models above $m_{\rm min}$ is appropriate for the determination of PL relationships.
- For a given Z, PL relationships derived on a mass range or period range restricted to a region near $m_{\rm min}$ (or to low periods) are much steeper than PL relationships derived over the whole mass range considered in the present paper. Thus, a *unique* linear least-square fit to the models down to $m_{\rm min}$ is not appropriate. Since the period at which the change of slope is expected depends on Z, the comparison of PL relationships derived on Cepheids observed near this critical P has to be taken with caution.
- The (linear) PL relationships derived in the present work from $m_{\rm min}$ to 12 $M_\odot$ show a weak dependence on metallicity, in agreement with a similar analysis performed by Saio and Gautschy (1998).
- A variation of Z from 0.02 to 0.004 on Period - Magnitude relationships yields a difference in magnitude at a given P of less than 0.12 mag in $VIJK$ bandpasses.
- A decrease of Z from 0.02 to 0.004 results in bluer $(B-V)$ colors by 0.1 - 0.12 mag at a given P, in agreement with observations. The effect of Z is found to be negligible for $(J-K)$. For $(V-K)$ colors, we find a small effect of Z (less than 0.06 mag) at a given P.
- For first overtone pulsators, the models predict also a change of slope at the low end of the PL distribution, due to the reduction of the He blue loop size. However, we expect this feature to be less pronounced than for F pulsators, due to the significant reduction of the 1H instability strip width (by more than 400 K), compared to the fundamental IS. According to the present standard models, the observed SMC 1H pulsators with log $P \lesssim 0$ should be in the first crossing phase. Because of their relatively large observed number, we suggest that first crossing models favor 1H as the dominant pulsating mode. Non-linear calculations should be able to test this hypothesis.
- The present standard models fail to reproduce the minimum periods observed in the LMC by the EROS and MACHO collaborations, and predict lower minimum periods. Models taking into account overshooting can better account for these observations, but they fail for the SMC Cepheids. Confirmation of the observed minimum periods in the MC by the forthcoming MACHO and OGLE data are urgently required to understand the source of this discrepancy.

The present conclusions regarding the metallicity effects remain valid for different treatments of convection used in the stellar models. We certainly acknowledge that the present results may be affected by the neglect of the pulsation-convection coupling. Since the present models yield general good agreement with different observations for *fundamental* pulsators, such approximation cannot be the source of severe shortcomings. For 1H pulsators however, we quote several discrepancies with observations, which may indicate that the neglect of pulsation-convection coupling is reasonable for the fundamental mode but not for overtones. This problem will be addressed in a forthcoming work.

Finally, the present work suggests that for samples of Cepheids with log $P \gtrsim 0.8$, metallicity effects are negligible for galactic and MC environments, and a universal PL relationship is certainly appropriate for the derivation of distance moduli. This work suggests also that observed PL relationships including low period Cepheids are to be taken with caution and should be avoided to derive distance moduli, since evolutionary effects break the linear form of this relationship at low P. The Z-effect suggested by Sasselov et al. (1997) in the low P regime is thus more likely the signature of these evolutionary effects.

Tables 6-8 are available by anonymous ftp:

```
ftp ftp.ens-lyon.fr
username: anonymous
ftp > cd /pub/users/CRAL/ibaraffe/cepheid
ftp > get ABHA98_models
ftp > quit
```

Special requests for models can be addressed to Y. Alibert.

Acknowledgements. We are grateful to our referee, A. Gautschy, for very pertinent comments and for improving the manuscript. We thank G. Chabrier for numerous discussions and for reading carefully the manuscript. We thank P. Fouqué for sending the filter transmission curves of the Carter System and for many interesting discussions. We thank also W. Glatzel for valuable discussions and U. Lee for providing the original pulsation code. Part of this work was performed during exchanges with the Universitäts-Sternwarte of Göttingen under APAPE support (PROCOPE contract 97151). The calculations were performed on the T3E at Centre d'Etudes Nucléaires de Grenoble.

References

Alcock, C., et al. 1998, AJ, in press, astro-ph/9811240

Alexander D. R., and Fergusson, J. W., 1994, ApJ, 437, 879

Allard, F., Hauschildt, P.H., Alexander, D.R., Starrfield, S., 1997, ARA&A, 35, 137

Baraffe, I., El Eid, M., 1991, A&A, 245, 548

Baraffe, I., Alibert, Y., Méra, D., Chabrier, G., Beaulieu, J-P., 1998, ApJ, 499, L205

Bauer, F., et al. 1998, A&A, submitted, astro-ph/9807094

Beaulieu, J.P., et al. 1995, A&A, 301, 137

Beaulieu, J.P., & Sasselov, D. 1996, 12th IAP Astr. meeting, "Astrophysical returns of microlensing surveys", eds R. Ferlet and JP. Maillard

Bersier, D., Burki, G., Kurucz, R.L., 1997, A&A, 320, 228

Bessell, M.S., 1990, PASP, 102, 1181

Bressan, F., Fagotto, G., Bertelli, G., & Chiosi, C. 1993, ApJS, 100, 674

Bono, G., Caputo, F., Castellani, V., Marconi, M., 1998a, preprint, astro-ph/9809127 (BCCM98)

Bono, G., Caputo, F., Marconi, M., 1998b, ApJ, 497, L43

Caldwell, J.A.R., Coulson, I.M. 1986, MNRAS, 218, 223

Chiosi, C., Wood, P.R., Capitanio, N., 1993, ApJS, 86, 541

de Jager, C., Nieuwenhuijzen, H., van der Hucht, K.A., 1988, A&AS, 72, 259

El Eid, M.F., 1994, MNRAS, 275, 983

Fernie, J.D., 1990, ApJ, 354, 295

Fry, A.M., Carney, B.W., 1997, AJ, 113, 1073

Gautschy, A., 1999, "Recent results onH_0", 19th Texas Symposium, Paris, astro-ph/9901021

Gieren, W.P., Barnes, T.G., Moffett, T.J., 1993, ApJ, 418, 135

Gieren, W.P., Fouqué, P., Gomez, M., 1998, ApJ, 496, 17, (GFG98)

Hauschildt, P.H., Allard, F., Baron, E., 1998, ApJ, in press

Huebner, W.F., Merts, H.L., Magee, H.N., Jr., Argo, M.F. 1977, Los Alamos Sci. Lab. Report LA 6760 MA

Iglesias, C.A., Rogers, F.J. 1991, ApJ, 371, L73

Iglesias, C.A., Rogers, F.J. 1996, ApJ, 464, 943

Iglesias, C.A., Rogers, F.J., Wilson, B. 1992, ApJ, 397, 717

Kippenhahn, R., Weigert, A. 1990, "Stellar Structure and Evolution", ed. M. Harvit, R. Kippenhahn, V. Trimble and J.P Zahn

Kollath, Z., Beaulieu, J-P., Buchler, J.R., Yecko, P., 1998, ApJ, 502, L55

Kudritzki, R.P., Pauldrach, A., Puls, J. 1987, A&A, 173, 293

Kudritzki, R.P., Pauldrach, A., Puls, J., Voels, S.R. 1991, "The Magellanic Clouds", IAU Symp. 148, ed. R.Haynes and D. milne, kluwer Acad. Publ., p. 279

Laney, C.D., Stobie, R.S. 1994, MNRAS, 266, 441 (LS94)

Lee, U. 1985, PASJ 37, 279

Leggett, S.K., 1992, ApJS, 82, 351

Morgan, S.M., Welch, D.L. 1997, AJ, 114, 1183

Pols, O.R., Schroder, K.P., Hurley, J.R., Tout, C.A., Eggleton, P.P., 1998, MNRAS, 298, 525

Renault, C., et al. 1996, 12th IAP Astr. meeting, "Astrophysical returns of microlensing surveys", eds R. Ferlet and JP. Maillard

Saio, H., Gautschy, A., 1998, ApJ, 498, 360

Sasselov, D., et al. 1997, A&A, 324, 471

Seaton, M.J., Yan., Y., Mihalas, D., Pradhan, A.K., 1994, MNRAS, 266, 805

Sekiguchi, M., Fukugita, M., 1997, The Observatory, 118, 73

Tanvir, N.R. 1997, Proceedings of the STScI May Symposium, "the Extragalactic Distance Scale", eds. M. Livio, M.Donahue and N. Panagia, p. 91

Udalski, A., Kubiak, M., Szymanski, M., 1997, AcA, 47, 319

Welch, D.L, et al. 1996, 12th IAP Astr. meeting, "Astrophysical returns of microlensing surveys", eds R. Ferlet and JP. Maillard

Yecko, P.A., Kollath, Z., Buchler, J.R., 1998, A&A, 336, 553

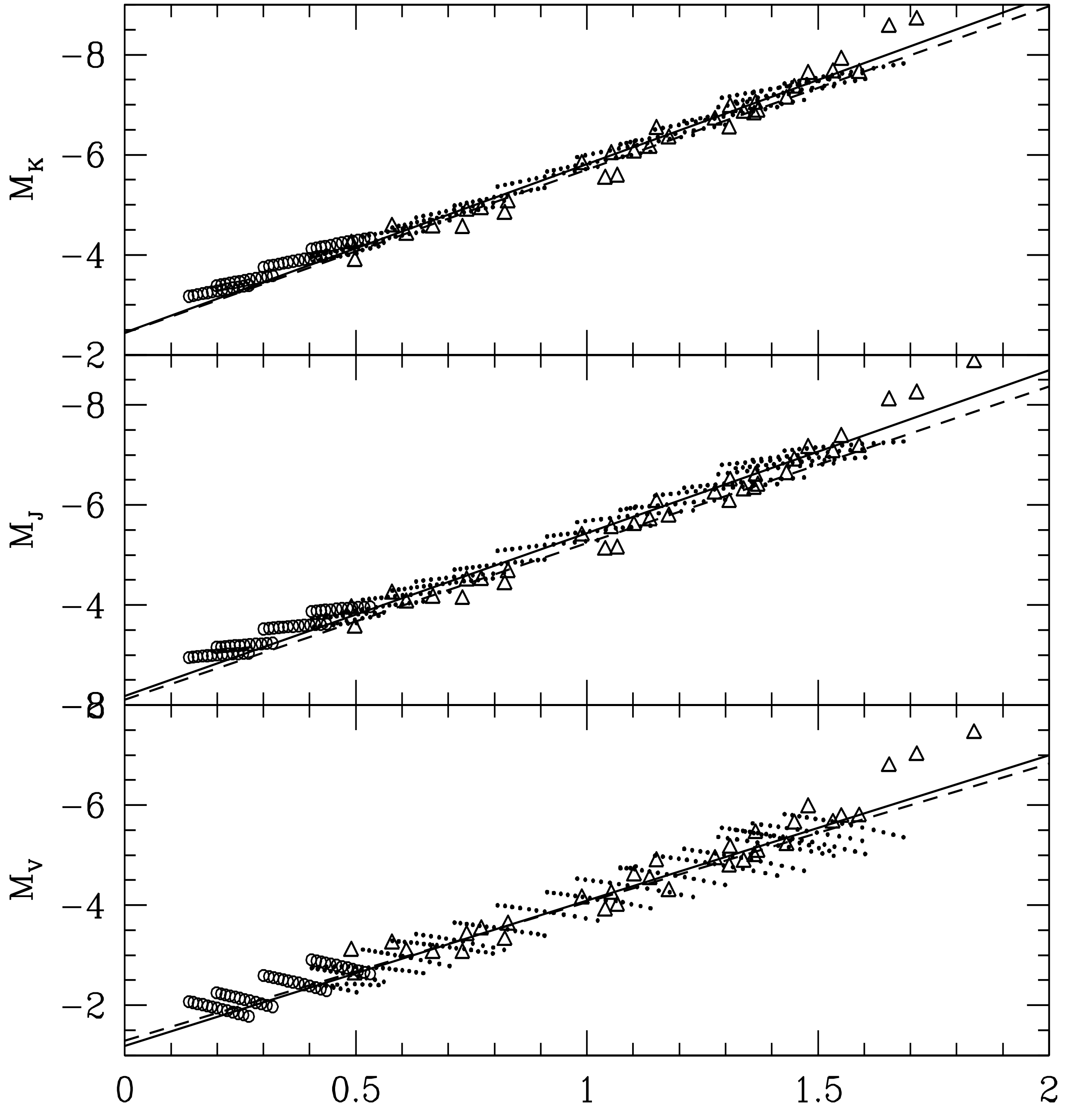

Fig. 11. Period - Magnitude diagrams in the VJK bands for solar metallicity standard models. The dots correspond to fundamental unstable modes during core He burning phase from $m_{\min} = 4.75\ M_\odot$ to $12\ M_\odot$. The open circles correspond to first crossing fundamental unstable modes for 4.75, 5, 5.5 and $6\ M_\odot$. Observations (open triangles) are from GFG98. The dashed curves correspond to the PL relationships given by GFG98. The solid curves correspond to the relationships derived from the present standard models.

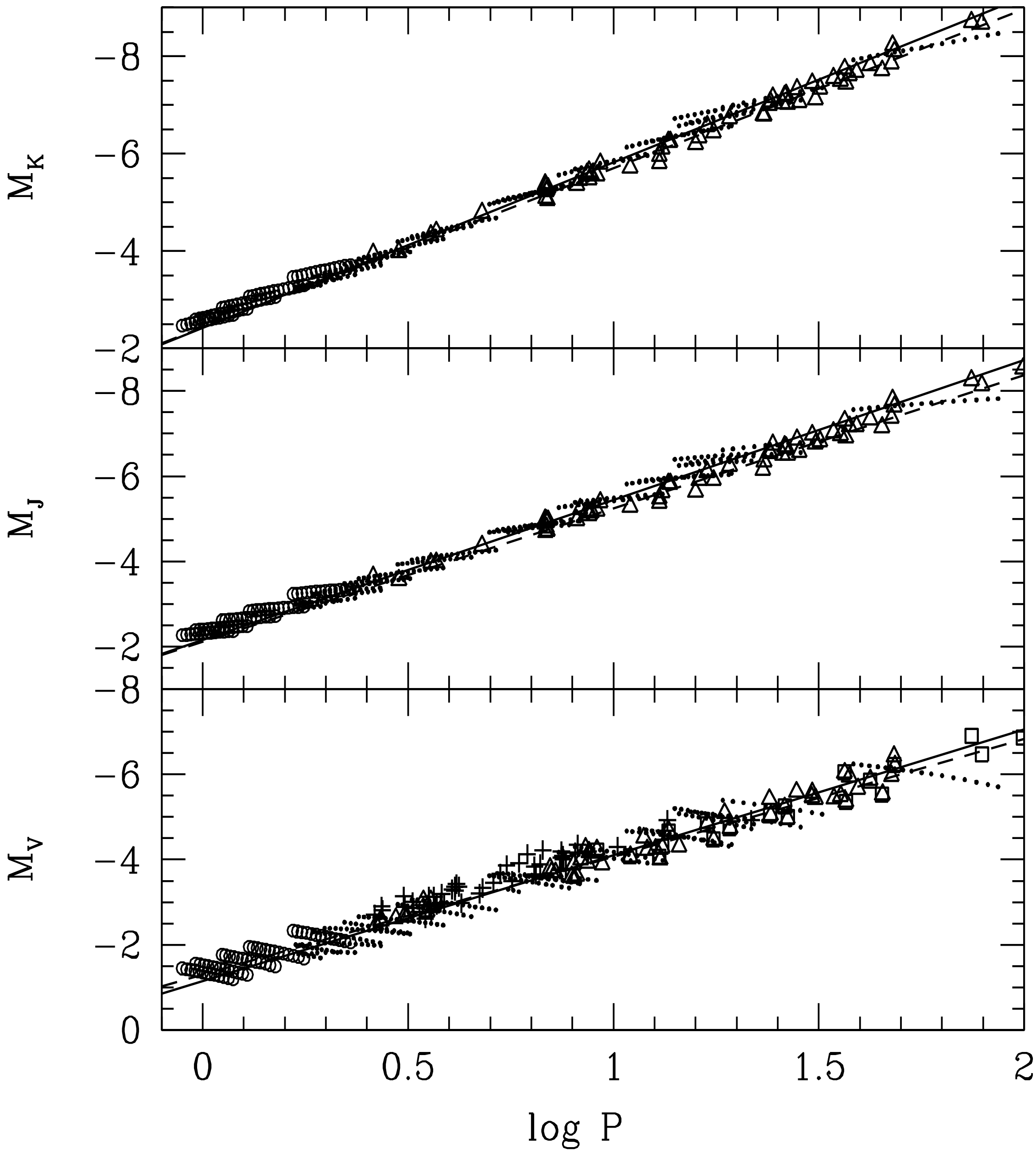

Fig. 12. Period - Magnitude diagrams in the *VJK* bands for standard models with Z=0.01 and LMC observed Cepheids. The dots correspond to fundamental unstable modes during core He burning phase from $m_{\rm min} = 3.875\ M_\odot$ to 12 $M_\odot$. The open circles correspond to first crossing fundamental unstable modes for 3.875, 4, 4.25, 4.5, 5 $M_\odot$. Observations are taken from GFG98 (open triangles), LS94 (open squares) and Sasselov et al. (1997) (+). The distance modulus is 18.50. The curves have the same meaning as in Fig. 11.

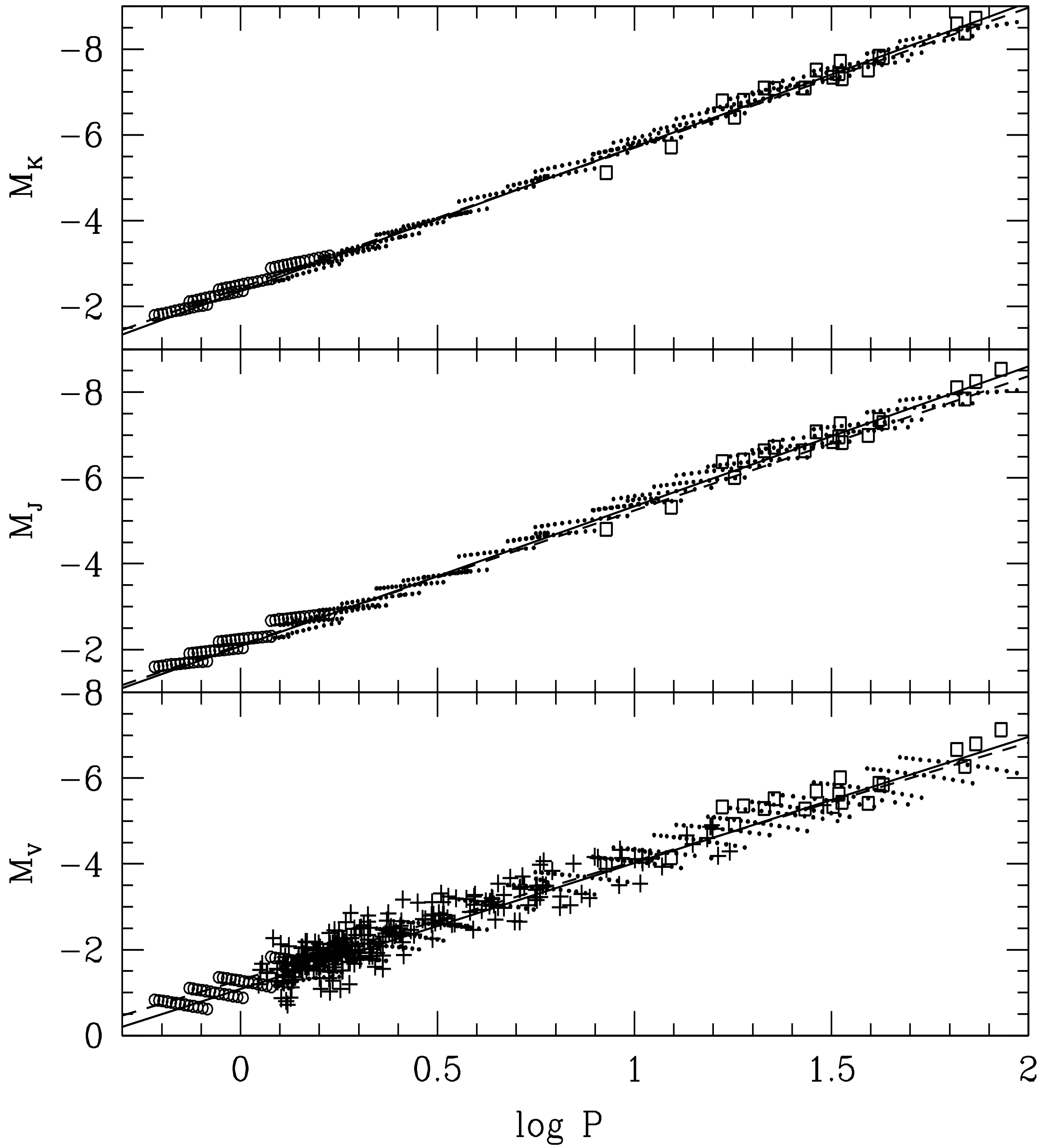

Fig. 13. Period - Magnitude diagrams in the VJK bands for standard models with Z=0.004 and SMC observed Cepheids. The dots correspond to fundamental unstable modes during core He burning phase from $m_{\min} = 3\ M_\odot$ to 12 $M_\odot$. The open circles correspond to first crossing fundamental unstable modes for 3, 3.25, 3.5 and 4 $M_\odot$. Observations are taken from LS94 (open squares) and Sasselov et al. (1997) (+). The distance modulus is 18.94. The curves have the same meaning as in Fig. 11.

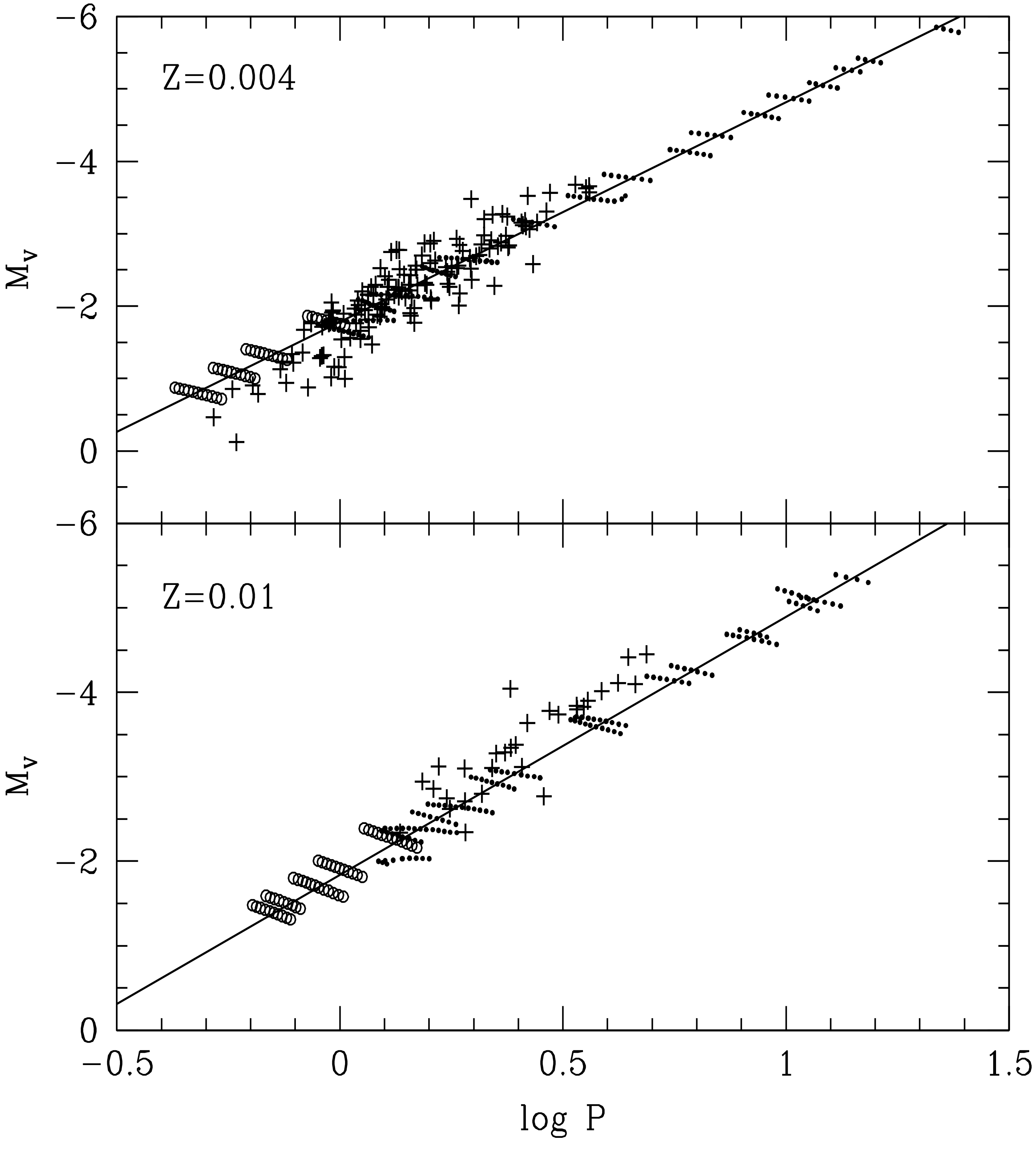

Fig. 14. Period - Magnitude diagram for 1H pulsators in the V band for standard models with Z=0.01 and the EROS LMC data (lower panel), and Z=0.004 and the EROS SMC data (upper panel). Symbols have the same meaning as in Fig. 12 for Z=0.01 and Fig. 13 for Z=0.004, but for 1H pulsators. The solid curves correspond to the P - $M_{\rm V}$ relationships derived from the models.

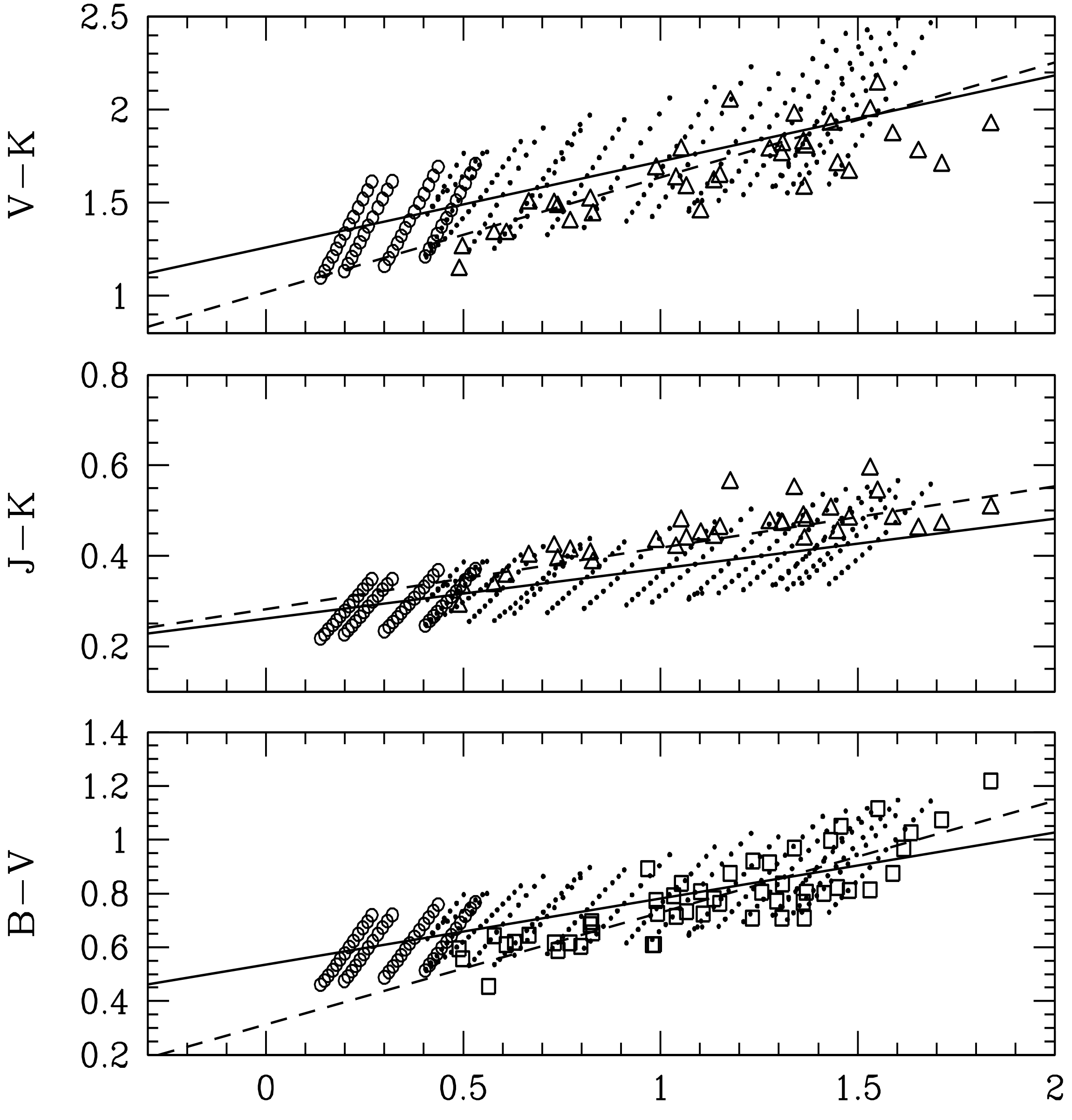

Fig. 15. Period - color diagrams for solar metallicity standard models and galactic Cepheids. The dots correspond to fundamental unstable modes during core He burning phase from $m_{\rm min} = 4.75\ M_\odot$ to 12 $M_\odot$. The open circles correspond to first crossing fundamental unstable modes (see Fig. 11 for the masses displayed). Observations are from GFG98 (open triangles) and LS94 (open squares). The dashed curves correspond to the PC relationships given by LS94. The solid curves correspond to the present PC relationships.

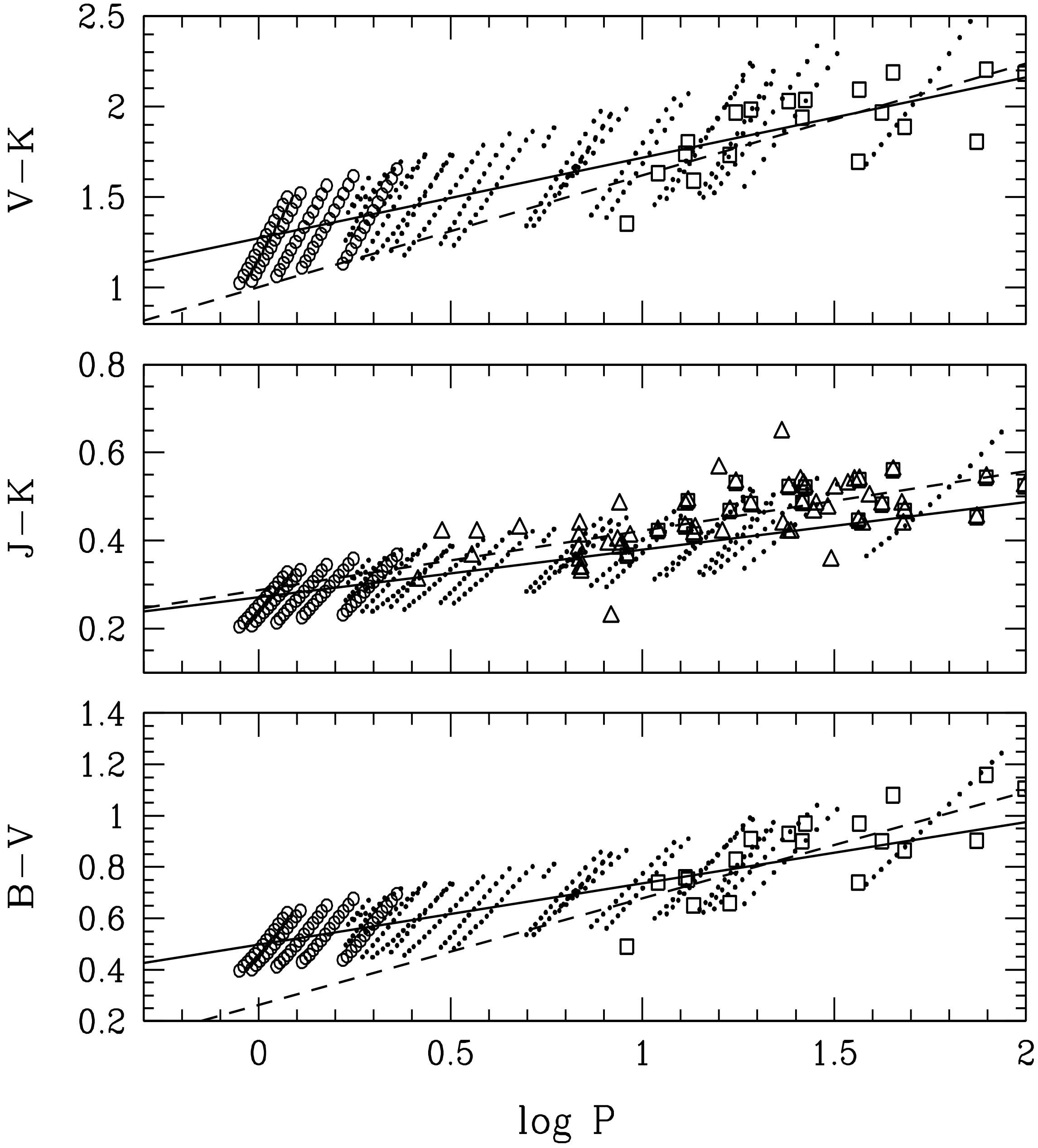

Fig. 16. Same as Fig. 15 for Z=0.01 standard models and LMC Cepheids. The dots correspond to fundamental unstable modes during core He burning phase from $m_{\rm min}$ = 3.875 $M_\odot$ to 12 $M_\odot$. The open circles correspond to first crossing fundamental unstable modes (see Fig. 12 for the masses displayed). Observations are from GFG98 (open triangles) and LS94 (open squares). The curves have the same meaning as in Fig. 15.

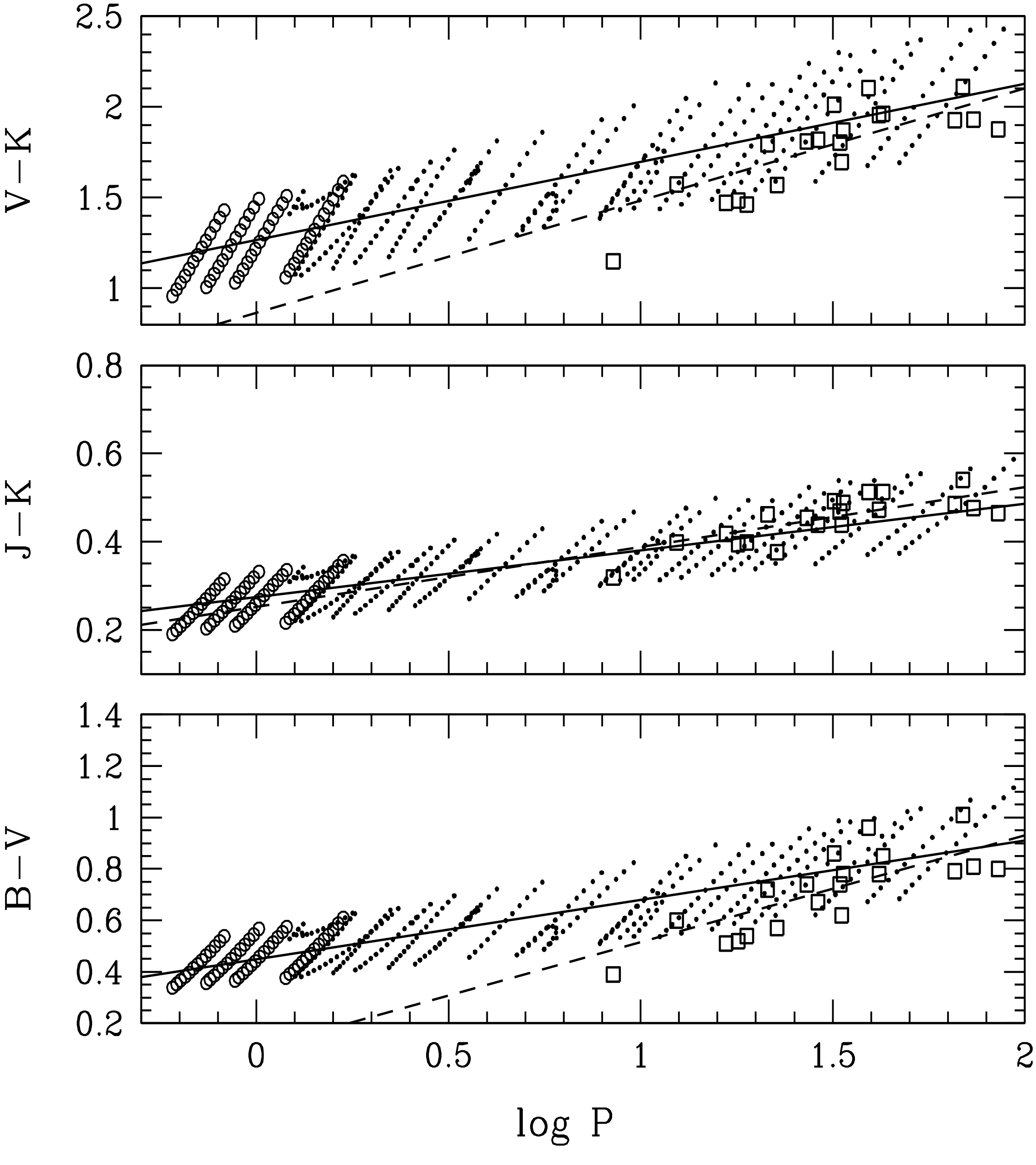

Fig. 17. Same as Fig. 15 for Z=0.004 standard models and SMC Cepheids. The dots correspond to fundamental unstable modes during core He burning phase from $m_{\rm min}$ = 3 $M_\odot$ to 12 $M_\odot$. The open circles correspond to first crossing fundamental unstable modes (see Fig. 13 for the masses displayed). Observations are from LS94 (open squares). The curves have the same meaning as in Fig. 15.

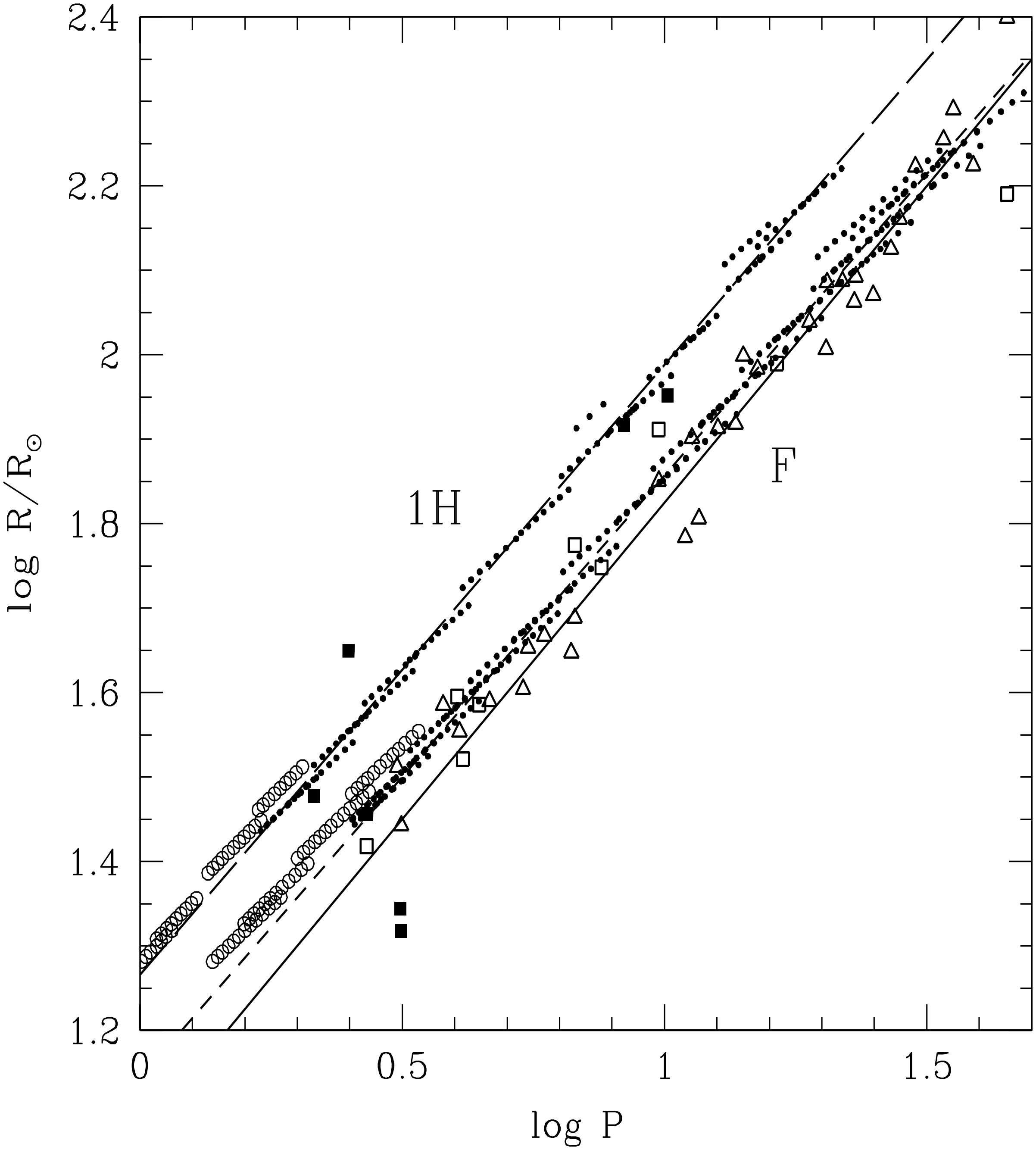

Fig. 18. Period - radius diagram for solar metallicity standard models and galactic Cepheids, for F (lower sequence) and 1H pulsators (upper sequence). Dots and open circles have the same meaning as in Fig. 11. Observations are from GFG98 (open triangles) and Bersier et al. (1997) for classical (open squares) and *s*- Cepheids (full squares). The solid curves correspond to the PR relationship given by GFG98. The dashed and long-dashed curves correspond to the present results for F and 1H pulsators respectively.

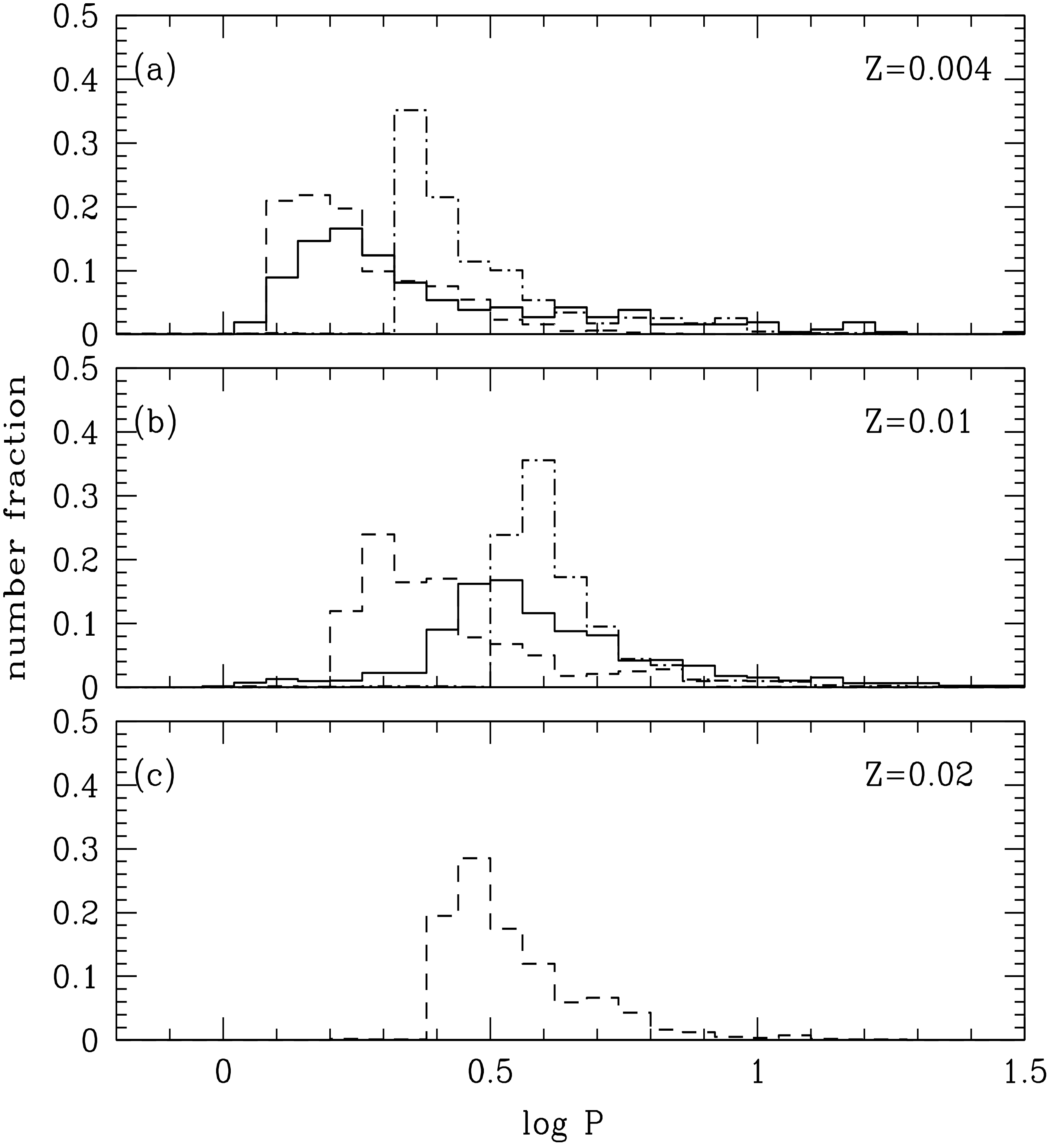

Fig. 19. **(a)**: Period-histogram for the SMC. The solid line corresponds to the EROS-1 observations (Sasselov et al. 1997). The dashed line corresponds to the present standard models for Z=0.004, and the dash-dotted line to models with overshooting. **(b):** same as (a) for LMC data and Z=0.01 models. The observed period-frequency distribution (solid line) is from MACHO (Alcock et al. 1998). **(c):** Same as (a) for Z=0.02 models.

Table 6. Standard models with $(Z,Y) = (0.02,\ 0.28)$. The mass m is in $M_\odot$; $T_{\rm eff}$ is the effective temperature in K; L corresponds to $\log L/L_\odot$; t is the age in units of 10^7 yrs; P_0 is the fundamental mode period in days. The BVI absolute magnitudes are given in the Johnson-Cousins system and the JHK magnitudes in the CIT system. For each mass, the blue (B) and red (R) edges are given during all crossings of the IS. For the first crossing, only models with $m \leq 6M_\odot$ are given.

edge	m	$T_{\rm eff}$	L	t	P_0	$M_{\rm B}$	$M_{\rm V}$	$M_{\rm I}$	$M_{\rm J}$	$M_{\rm H}$	$M_{\rm K}$
B	4.750	6304.7	2.710	9.8144	1.38	-1.61	-2.07	-2.63	-2.95	-3.16	-3.17
R	4.750	5528.6	2.634	9.8184	1.86	-1.06	-1.78	-2.55	-3.04	-3.36	-3.39
R	4.737	5331.8	2.848	10.9081	3.17	-1.46	-2.26	-3.10	-3.64	-3.99	-4.03
B	4.737	5764.5	2.879	10.9573	2.57	-1.80	-2.43	-3.13	-3.57	-3.84	-3.87
R	4.737	5332.4	2.905	11.5683	3.54	-1.61	-2.40	-3.24	-3.78	-4.13	-4.17
B	5.000	6240.8	2.782	8.6764	1.58	-1.77	-2.25	-2.82	-3.15	-3.37	-3.38
R	5.000	5526.1	2.713	8.6793	2.09	-1.25	-1.97	-2.74	-3.24	-3.56	-3.59
R	4.985	5323.1	2.933	9.6454	3.64	-1.67	-2.47	-3.31	-3.85	-4.21	-4.24
B	4.985	6089.2	2.986	9.6985	2.54	-2.22	-2.74	-3.35	-3.72	-3.94	-3.96
B	4.985	6107.2	2.994	9.7986	2.55	-2.25	-2.76	-3.36	-3.73	-3.95	-3.97
R	4.984	5253.6	3.010	10.4325	4.42	-1.81	-2.64	-3.50	-4.07	-4.43	-4.47
B	5.500	6188.4	2.922	6.8681	2.00	-2.10	-2.59	-3.17	-3.52	-3.74	-3.75
R	5.500	5423.5	2.851	6.8702	2.73	-1.53	-2.29	-3.10	-3.62	-3.95	-3.99
R	5.477	5167.8	3.079	7.6340	5.04	-1.92	-2.79	-3.68	-4.27	-4.65	-4.69
B	5.477	6042.6	3.136	7.6759	3.28	-2.58	-3.11	-3.73	-4.10	-4.34	-4.36
B	5.476	6027.6	3.208	8.2280	3.79	-2.75	-3.29	-3.91	-4.29	-4.52	-4.54
R	5.476	5147.6	3.182	8.3847	6.26	-2.16	-3.03	-3.93	-4.53	-4.91	-4.95
B	6.000	6105.0	3.051	5.6114	2.53	-2.39	-2.91	-3.51	-3.87	-4.10	-4.12
R	6.000	5403.3	2.987	5.6127	3.40	-1.86	-2.63	-3.44	-3.96	-4.30	-4.34
R	5.965	5090.6	3.219	6.2371	6.62	-2.21	-3.11	-4.03	-4.64	-5.03	-5.08
B	5.965	5928.8	3.268	6.2627	4.27	-2.85	-3.43	-4.07	-4.47	-4.72	-4.75
B	5.963	5911.4	3.361	6.8159	5.17	-3.08	-3.65	-4.31	-4.71	-4.96	-4.98
R	5.963	5116.4	3.331	6.8683	8.10	-2.51	-3.39	-4.30	-4.91	-5.30	-5.34
R	6.932	4988.2	3.470	4.3770	10.55	-2.75	-3.70	-4.65	-5.30	-5.71	-5.76
B	6.932	5852.1	3.503	4.3831	6.41	-3.40	-4.00	-4.67	-5.08	-5.34	-5.37
B	6.927	5799.5	3.613	4.8696	8.20	-3.65	-4.26	-4.95	-5.37	-5.64	-5.66
R	6.927	4930.9	3.579	4.8845	13.72	-2.97	-3.94	-4.92	-5.58	-6.01	-6.06
R	7.886	4821.3	3.689	3.2799	16.98	-3.14	-4.17	-5.19	-5.89	-6.34	-6.40
B	7.886	5764.9	3.722	3.2818	9.53	-3.90	-4.53	-5.22	-5.66	-5.92	-5.95
B	7.876	5722.8	3.817	3.6870	11.80	-4.11	-4.75	-5.46	-5.91	-6.18	-6.21
R	7.876	4859.0	3.781	3.6907	19.91	-3.39	-4.40	-5.41	-6.11	-6.54	-6.60
R	8.835	4700.2	3.888	2.5871	25.80	-3.50	-4.59	-5.67	-6.42	-6.88	-6.95
B	8.835	5642.7	3.918	2.5880	14.04	-4.31	-4.99	-5.72	-6.18	-6.47	-6.50
B	8.819	5601.2	3.977	2.8848	16.23	-4.43	-5.12	-5.87	-6.34	-6.63	-6.67
R	8.818	4660.5	3.935	2.8870	29.49	-3.58	-4.69	-5.78	-6.55	-7.02	-7.10
R	9.822	4680.3	4.053	2.0969	34.18	-3.89	-4.99	-6.07	-6.83	-7.30	-7.37
B	9.822	5543.9	4.080	2.0973	19.24	-4.64	-5.36	-6.13	-6.62	-6.92	-6.95
B	9.791	5585.4	4.135	2.3821	20.99	-4.81	-5.51	-6.26	-6.74	-7.03	-7.06
R	9.790	4589.3	4.089	2.3835	40.00	-3.88	-5.02	-6.15	-6.95	-7.43	-7.51
R	10.883	4713.5	4.171	1.7332	39.41	-4.20	-5.29	-6.36	-7.11	-7.57	-7.64
B	10.883	5521.4	4.193	1.7334	22.84	-4.91	-5.64	-6.41	-6.90	-7.20	-7.24
B	10.826	5523.0	4.268	2.0405	26.77	-5.09	-5.82	-6.59	-7.08	-7.39	-7.42
R	10.825	4610.3	4.224	2.0412	48.41	-4.22	-5.36	-6.48	-7.27	-7.75	-7.83
B	11.940	5539.3	4.154	1.4633	19.59	-4.83	-5.55	-6.32	-6.80	-7.10	-7.14
R	11.940	4643.6	4.098	1.4635	33.45	-3.97	-5.08	-6.18	-6.96	-7.43	-7.51

Table 7. Same as in Table 6 for standard models with $(Z, Y) = (0.01,\ 0.25)$. For the first crossing, only models with $m \leq 5M_\odot$ are given.

edge	m	$T_{\rm eff}$	L	t	P_0	$M_{\rm B}$	$M_{\rm V}$	$M_{\rm I}$	$M_{\rm J}$	$M_{\rm H}$	$M_{\rm K}$
B	3.875	6466.1	2.463	16.2120	0.89	-1.05	-1.45	-1.96	-2.27	-2.46	-2.47
R	3.875	5703.9	2.394	16.2201	1.19	-0.57	-1.19	-1.91	-2.37	-2.67	-2.69
R	3.870	5552.6	2.605	18.2885	1.94	-1.02	-1.69	-2.45	-2.94	-3.27	-3.30
B	3.870	5819.8	2.625	18.3646	1.71	-1.21	-1.79	-2.47	-2.90	-3.18	-3.20
R	3.870	5431.9	2.665	19.5117	2.35	-1.10	-1.82	-2.61	-3.14	-3.48	-3.51
B	4.000	6441.0	2.507	15.0811	0.96	-1.15	-1.55	-2.07	-2.39	-2.59	-2.59
R	4.000	5674.2	2.437	15.0882	1.28	-0.67	-1.30	-2.02	-2.48	-2.79	-2.82
R	3.995	5528.2	2.658	17.0054	2.13	-1.14	-1.82	-2.58	-3.08	-3.41	-3.44
B	3.995	6055.4	2.698	17.1486	1.69	-1.50	-2.00	-2.61	-3.00	-3.24	-3.26
R	3.995	5380.8	2.734	18.3635	2.71	-1.24	-1.98	-2.79	-3.33	-3.68	-3.71
B	4.250	6389.9	2.592	12.8715	1.11	-1.35	-1.77	-2.30	-2.62	-2.82	-2.83
R	4.250	5610.9	2.521	12.8769	1.50	-0.85	-1.50	-2.23	-2.72	-3.03	-3.06
R	4.244	5396.6	2.758	14.7441	2.70	-1.31	-2.04	-2.85	-3.38	-3.73	-3.77
B	4.244	6207.4	2.815	14.8887	1.86	-1.86	-2.31	-2.88	-3.23	-3.46	-3.47
B	4.244	6209.4	2.848	15.3763	1.98	-1.94	-2.39	-2.96	-3.31	-3.54	-3.55
R	4.244	5385.5	2.842	15.9089	3.20	-1.52	-2.25	-3.06	-3.59	-3.95	-3.98
B	4.500	6309.4	2.670	11.1956	1.30	-1.52	-1.95	-2.50	-2.84	-3.05	-3.06
R	4.500	5539.0	2.600	11.1998	1.76	-1.00	-1.68	-2.44	-2.94	-3.27	-3.30
R	4.493	5381.4	2.852	12.8880	3.15	-1.54	-2.28	-3.08	-3.62	-3.98	-4.01
B	4.493	6138.6	2.905	13.0236	2.21	-2.06	-2.53	-3.11	-3.48	-3.71	-3.73
B	4.493	6174.1	2.957	13.6604	2.40	-2.20	-2.66	-3.24	-3.60	-3.83	-3.84
R	4.493	5315.9	2.933	13.9023	3.85	-1.70	-2.46	-3.29	-3.84	-4.21	-4.25
B	5.000	6265.6	2.823	8.7200	1.66	-1.89	-2.33	-2.89	-3.23	-3.45	-3.46
R	5.000	5487.8	2.757	8.7227	2.29	-1.36	-2.06	-2.83	-3.35	-3.68	-3.71
R	4.990	5237.9	3.022	10.0765	4.51	-1.87	-2.66	-3.52	-4.09	-4.47	-4.51
B	4.990	6071.5	3.077	10.2079	2.98	-2.46	-2.95	-3.55	-3.93	-4.17	-4.19
B	4.990	6081.7	3.121	10.6372	3.23	-2.58	-3.06	-3.66	-4.04	-4.28	-4.29
R	4.990	5221.5	3.088	10.7208	5.17	-2.02	-2.82	-3.68	-4.26	-4.64	-4.68
R	5.977	5093.5	3.312	6.6542	7.79	-2.48	-3.33	-4.24	-4.86	-5.27	-5.31
B	5.976	5910.4	3.356	6.7416	4.99	-3.09	-3.62	-4.27	-4.68	-4.94	-4.97
B	5.976	5908.7	3.378	6.9163	5.22	-3.14	-3.68	-4.33	-4.74	-5.00	-5.02
R	5.975	5112.1	3.350	6.9730	8.28	-2.58	-3.43	-4.34	-4.95	-5.35	-5.39
R	6.954	5015.4	3.557	4.6978	12.09	-3.02	-3.92	-4.85	-5.49	-5.92	-5.96
B	6.954	5818.6	3.579	4.7019	7.36	-3.60	-4.17	-4.84	-5.27	-5.54	-5.57
B	6.952	5835.8	3.630	5.0668	8.07	-3.73	-4.30	-4.96	-5.39	-5.66	-5.68
R	6.952	4985.1	3.589	5.0695	13.19	-3.07	-3.98	-4.93	-5.58	-6.01	-6.05
R	7.921	4834.5	3.767	3.5386	19.40	-3.37	-4.36	-5.36	-6.07	-6.53	-6.58
B	7.921	5731.7	3.788	3.5400	10.77	-4.07	-4.67	-5.37	-5.82	-6.10	-6.13
B	7.918	5686.2	3.811	3.8251	11.58	-4.10	-4.72	-5.43	-5.89	-6.18	-6.21
R	7.918	4818.1	3.751	3.8262	19.09	-3.32	-4.31	-5.33	-6.04	-6.50	-6.55
R	8.880	4731.2	3.953	2.8145	28.55	-3.72	-4.76	-5.82	-6.56	-7.04	-7.10
B	8.879	5640.2	3.978	2.8152	15.41	-4.49	-5.12	-5.85	-6.32	-6.62	-6.65
B	8.873	5673.1	3.956	3.0381	14.45	-4.45	-5.08	-5.79	-6.25	-6.54	-6.58
R	8.873	4932.3	3.899	3.0386	21.65	-3.78	-4.72	-5.69	-6.36	-6.80	-6.85
R	9.930	4769.9	4.068	2.2168	32.22	-4.04	-5.07	-6.10	-6.83	-7.30	-7.36
B	9.930	5590.1	4.090	2.2171	18.46	-4.73	-5.39	-6.13	-6.61	-6.92	-6.95
B	10.979	5643.9	4.007	1.8114	14.11	-4.57	-5.20	-5.92	-6.39	-6.69	-6.72
R	10.979	4861.9	3.954	1.8115	21.96	-3.86	-4.83	-5.83	-6.53	-6.98	-7.03
B	11.874	5429.4	4.454	1.8127	38.40	-5.51	-6.24	-7.04	-7.56	-7.89	-7.93
R	11.868	4392.1	4.430	1.8160	86.39	-4.47	-5.71	-6.94	-7.82	-8.37	-8.47

Table 8. Same as in Table 6 for standard models with $(Z, Y) = (0.004, 0.25)$. For the first crossing, only models with $m \leq 4M_\odot$ are given

edge	m	$T_{\rm eff}$	L	t	P_0	$M_{\rm B}$	$M_{\rm V}$	$M_{\rm I}$	$M_{\rm J}$	$M_{\rm H}$	$M_{\rm K}$
B	3.000	6631.0	2.225	26.0600	0.60	-0.49	-0.83	-1.31	-1.60	-1.79	-1.79
R	3.000	5837.0	2.166	26.0772	0.82	-0.08	-0.62	-1.29	-1.73	-2.03	-2.05
R	2.998	5679.9	2.370	29.3156	1.32	-0.52	-1.11	-1.83	-2.30	-2.62	-2.64
B	2.998	5858.8	2.384	29.4170	1.22	-0.64	-1.17	-1.83	-2.27	-2.56	-2.58
R	2.998	5550.5	2.483	32.0947	1.78	-0.74	-1.37	-2.12	-2.63	-2.97	-2.99
B	3.250	6534.5	2.335	21.4880	0.74	-0.74	-1.10	-1.60	-1.90	-2.10	-2.11
R	3.250	5741.4	2.273	21.4996	1.02	-0.31	-0.88	-1.58	-2.04	-2.35	-2.37
R	3.248	5556.0	2.520	24.7568	1.81	-0.84	-1.46	-2.21	-2.72	-3.06	-3.08
B	3.248	6389.0	2.582	25.2131	1.26	-1.33	-1.71	-2.24	-2.57	-2.79	-2.79
B	3.248	6396.7	2.603	25.6821	1.31	-1.39	-1.77	-2.29	-2.62	-2.84	-2.84
R	3.248	5496.7	2.637	27.0614	2.34	-1.10	-1.74	-2.51	-3.03	-3.37	-3.40
B	3.500	6485.7	2.438	17.9419	0.88	-0.99	-1.36	-1.87	-2.18	-2.38	-2.39
R	3.500	5716.3	2.379	17.9499	1.20	-0.56	-1.14	-1.84	-2.31	-2.62	-2.64
R	3.498	5514.7	2.643	20.7979	2.23	-1.12	-1.76	-2.53	-3.04	-3.38	-3.41
B	3.498	6326.6	2.711	21.3714	1.59	-1.64	-2.03	-2.57	-2.91	-3.13	-3.14
B	3.498	6269.9	2.765	22.3496	1.81	-1.75	-2.16	-2.72	-3.07	-3.29	-3.30
R	3.498	5449.5	2.747	22.5792	2.84	-1.35	-2.01	-2.79	-3.32	-3.67	-3.70
B	4.000	6424.4	2.628	13.0369	1.19	-1.46	-1.83	-2.35	-2.68	-2.89	-2.89
R	4.000	5601.6	2.567	13.0418	1.69	-0.98	-1.59	-2.33	-2.82	-3.15	-3.18
R	3.998	5362.6	2.835	14.9299	3.27	-1.51	-2.21	-3.02	-3.57	-3.94	-3.97
B	3.998	6212.6	2.899	15.3241	2.21	-2.08	-2.49	-3.06	-3.42	-3.65	-3.67
B	3.998	6151.7	2.964	16.2167	2.59	-2.22	-2.65	-3.23	-3.60	-3.84	-3.86
R	3.998	5297.1	2.944	16.3816	4.23	-1.74	-2.47	-3.30	-3.86	-4.24	-4.28
R	4.997	5237.8	3.140	8.5581	5.55	-2.19	-2.94	-3.79	-4.37	-4.76	-4.80
B	4.997	6043.7	3.176	8.6299	3.58	-2.71	-3.17	-3.78	-4.17	-4.43	-4.44
B	4.997	6003.3	3.313	9.6985	4.77	-3.04	-3.51	-4.12	-4.52	-4.78	-4.80
R	4.997	5156.7	3.290	9.7818	7.92	-2.50	-3.29	-4.17	-4.77	-5.18	-5.22
R	5.995	5069.4	3.417	5.6779	9.59	-2.75	-3.58	-4.49	-5.12	-5.54	-5.58
B	5.995	5932.8	3.436	5.6864	5.60	-3.32	-3.80	-4.44	-4.86	-5.12	-5.14
B	5.994	5832.6	3.581	6.5151	7.88	-3.63	-4.15	-4.81	-5.25	-5.53	-5.55
R	5.993	5024.9	3.556	6.5638	13.12	-3.05	-3.90	-4.83	-5.47	-5.91	-5.95
R	6.988	4937.2	3.664	4.1333	15.67	-3.24	-4.14	-5.10	-5.77	-6.22	-6.27
B	6.988	5787.3	3.677	4.1355	8.84	-3.85	-4.39	-5.06	-5.51	-5.79	-5.82
B	6.986	5777.6	3.795	4.7436	11.22	-4.14	-4.67	-5.35	-5.80	-6.09	-6.11
R	6.986	4947.7	3.763	4.7451	19.06	-3.49	-4.38	-5.34	-6.01	-6.46	-6.50
R	7.977	4945.3	3.881	3.2176	22.02	-3.78	-4.67	-5.64	-6.30	-6.75	-6.80
B	7.977	5740.7	3.894	3.2185	12.77	-4.36	-4.91	-5.60	-6.06	-6.35	-6.38
B	7.972	5701.6	3.972	3.6736	15.35	-4.53	-5.10	-5.80	-6.26	-6.56	-6.59
R	7.972	4829.4	3.938	3.6745	27.44	-3.81	-4.77	-5.78	-6.48	-6.95	-7.00
R	8.972	4772.5	4.043	2.5642	32.77	-4.01	-5.00	-6.03	-6.76	-7.24	-7.30
B	8.972	5641.5	4.059	2.5647	17.52	-4.72	-5.31	-6.03	-6.50	-6.81	-6.84
B	8.964	5625.3	4.117	2.9297	19.90	-4.85	-5.44	-6.17	-6.65	-6.96	-6.99
R	8.964	4786.1	4.081	2.9303	35.16	-4.11	-5.10	-6.13	-6.85	-7.33	-7.38
R	9.987	4767.9	4.181	2.0752	40.58	-4.33	-5.33	-6.37	-7.10	-7.58	-7.64
B	9.987	5564.1	4.193	2.0755	22.46	-5.00	-5.62	-6.37	-6.86	-7.18	-7.21
B	9.962	5562.2	4.307	2.4855	28.54	-5.28	-5.90	-6.64	-7.14	-7.46	-7.49
R	9.962	4713.1	4.283	2.4864	53.56	-4.51	-5.54	-6.61	-7.36	-7.86	-7.91
B	10.938	5450.5	4.450	2.1391	38.98	-5.55	-6.22	-7.01	-7.53	-7.86	-7.90
R	10.937	4669.6	4.433	2.1403	72.15	-4.81	-5.88	-6.97	-7.74	-8.24	-8.30
B	11.912	5428.8	4.562	1.8561	47.16	-5.80	-6.49	-7.28	-7.81	-8.14	-8.18
R	11.909	4596.2	4.548	1.8585	93.53	-5.01	-6.12	-7.25	-8.04	-8.57	-8.63